

ZeroDVFS: Zero-Shot LLM-Guided Core and Frequency Allocation for Embedded Platforms

Mohammad Pivezhandi¹, Mahdi Banisharif², Abusayeed Saifullah³, and Ali Jannesari²

¹Wayne State University

²Iowa State University

³The University of Texas at Dallas

Abstract

Dynamic voltage and frequency scaling (DVFS) and task-to-core allocation are critical for thermal management and balancing energy and performance in embedded systems. Existing approaches either rely on utilization-based heuristics that overlook stall times, or require extensive offline profiling for table generation, preventing runtime adaptation. We propose a model-based hierarchical multi-agent reinforcement learning (MARL) framework for thermal- and energy-aware scheduling on multi-core platforms. Two collaborative agents decompose the exponential action space, achieving 358ms latency for subsequent decisions. First decisions require 3.5 to 8.0s including one-time LLM feature extraction. An accurate environment model leverages regression techniques to predict thermal dynamics and performance states. When combined with LLM-extracted semantic features, the environment model enables zero-shot deployment for new workloads on trained platforms by generating synthetic training data without requiring workload-specific profiling samples. We introduce LLM-based semantic feature extraction that characterizes OpenMP programs through 13 code-level features without execution. The Dyna-Q-inspired framework integrates direct reinforcement learning with model-based planning, achieving 20 \times faster convergence than model-free methods. Experiments on BOTS and PolybenchC benchmarks across NVIDIA Jetson TX2, Jetson Orin NX, RubikPi, and Intel Core i7 demonstrate 7.09 \times better energy efficiency and 4.0 \times better makespan than Linux ondemand governor. First-decision latency is 8,300\$ times\$ faster than table-based profiling, enabling practical deployment in dynamic embedded systems.

1 Introduction

Energy-efficient embedded systems are limited by computational resources and play a crucial role in various applications, including IoT devices, wearable electronics, and autonomous vehicles. In these systems, managing the thermal dynamics prevents thermal overheating, ensures system reliability, and avoids non-uniform aging due to uneven workload distribution among the cores [9, 19]. However, the available thermal-aware energy-efficient methods proposed for embedded systems lack scalability to many cores and adaptability to different platforms, especially in dynamic and resource-constrained environments, and often incur prohibitive computational overhead. Complementary approaches in the literature address related challenges through hierarchical multi-agent scheduling, statistical feature-aware task allocation, few-shot reinforcement learning, and graph-driven performance modeling.

Dynamic Voltage and Frequency Scaling (DVFS) allows for runtime adjustment of voltage and frequency levels, balancing temperature and performance. Besides, an intelligent task migration and load balancing based on the operating system kernel helps redistribute computational tasks to avoid localized thermal hotspots. However, existing open-loop governors often prove inadequate in addressing the per-core frequency adjustments based on thermal behavior within embedded environments [19]. A feedback control technique can augment these methods by proactively tracking the temperature fluctuations and

limiting the impact of thermal escalation [48, 41]. Various feedback-based algorithms based on meta-heuristics, integer programming, and machine learning have been proposed [70, 67, 79, 29, 37, 38, 30], but these approaches lack application-agnostic or computationally efficient structures for adaptation in real-time systems.

Given the complexity of embedded systems, the cost-intensive nature of collecting real-world data adds to the challenges of task and processor profiling. This complexity frequently leads to unpredictable execution time estimates, aggravated by limited hardware feedback mechanisms within these systems. These challenges can significantly hinder efficient core allocation, affecting overall performance and energy efficiency. Consequently, existing task scheduling strategies mostly prioritize workload demand or only utilization metrics over temperature and system-related considerations. This trend is discernible in Linux kernel governors [9] and recently formulated policies [38, 30, 41]. Consequently, these strategies often overlook detailed insights provided by system profilers during task execution [3] and allocate resource-intensive tasks to hot cores, which are more sensitive to temperature elevations. State-of-the-art heuristic approaches like the precise scheduler [7] achieve near-optimal energy efficiency for static frequency assignment through exhaustive offline profiling across all configurations, but require 8 to 12 hours of table generation per benchmark (e.g., profiling a 1 to 5 second task across all core-frequency combinations with multiple repetitions), preventing runtime adaptation. Their static nature limits adaptability to thermal variations and workload phase changes.

Model-based reinforcement learning (RL) uses a predictive model to simulate future states and make informed decisions, enhancing the adaptability and efficiency of embedded systems. Having a model of the environment helps to adapt to new tasks with minimal data, and is particularly beneficial for embedded systems with limited computational resources and varying workloads. For example, automotive systems using multi-agent RL (MARL) can converge the DVFS strategies faster by each agent getting feedback from real-data and inference from the model of the processor, ensuring energy-efficient and reliable performance for safety-critical tasks. In mobile devices, the environment model combined with LLM-extracted semantic features enables zero-shot deployment: RL agents can be trained using synthetic data generated by the model without requiring any profiling samples from the target platform. This eliminates the sample collection overhead that limits prior transfer learning approaches. Critically, model-based approaches enable low-latency decision-making by amortizing learning costs across multiple decisions. First decisions on new benchmarks require 3.5 to 8.0s including one-time LLM feature extraction, while subsequent decisions achieve 358ms. First-decision latency is 8,300\$ times\$ faster than exhaustive table-based profiling.

This paper introduces a thermal-aware model-based Multi-Agent Reinforcement Learning (MARL) approach to enhance energy efficiency in embedded systems with minimal real-data requirements. These MARL techniques enable collaborative decision-making among multiple agents to optimize system performance while considering thermal constraints [33]. The key objectives of our work are threefold: first, to develop a thermal-aware modeling framework that captures the thermal dynamics of embedded systems under varying workloads and environmental conditions; second, to integrate this modeling framework with zero-shot deployment techniques through an off-policy MARL approach to enable efficient adaptation to new platforms with zero profiling samples from target hardware; and third, to evaluate the effectiveness of the proposed approach in optimizing thermal management and improving energy efficiency in real-world embedded systems, with emphasis on decision latency and makespan improvement of $4.0\times$ compared to exhaustive table-based and heuristic methods.

The proposed thermal-aware modeling approach augments the sample space by leveraging planning on trained models based on accurate data, contrary to previously proposed approaches based on direct Reinforcement Learning (RL) [61, 33, 43, 42]. Several multivariate regression model architectures are tuned, and exploration is done to select the computationally efficient models concerning low overhead and high accuracy. The proposed models outperform the accuracy of the state-of-the-art temperature modeling heuristics [25], achieving over $6\times$ better temperature prediction accuracy while maintaining model inference latencies under 5ms.

Through extensive experimentation and evaluation on representative embedded system platforms, we

demonstrate the effectiveness of the proposed approach in achieving thermal awareness, energy efficiency, and system reliability. Several low-energy methodologies are implemented including single-agent and multi-agent direct RL and model-based RL, to be compared with federated energy-aware scheduling [7] and linux governors [9]. Our framework integrates runtime monitoring of temperature patterns using Linux in-kernel profiling and the Barcelona OpenMP Tasks Suite (BOTS) and PolybenchC for workload characterization [20]. By leveraging the capabilities of MARL, our approach offers a flexible and adaptive solution for zero-shot deployment of temperature-aware and energy-efficient scheduling on new embedded systems, paving the way for enhanced performance and sustainability in a wide range of applications such as mobile and autonomous systems.

The key contributions of the paper are as follows:

1. The modeling framework is integrated into the few-shot learning techniques through an off-policy MARL approach to enable efficient adaptation to new thermal scenarios with limited training data. Two separate temperature and profiler agents cooperate to increase the action space for thermal awareness and energy efficiency. A goal-based reward function based on makespan, power consumption, and temperature deviation is provided.
2. We developed a thermal-aware accurate modeling framework to capture the thermal dynamics of the embedded processors under varying workloads and environmental conditions. The precise modeling framework reduces the sample collection overhead, achieving $4.0 \times$ better mean makespan compared to heuristic baselines while converging $20 \times$ faster than model-free methods.
3. We introduce LLM-based semantic feature extraction that characterizes OpenMP programs through 13 code-level features without execution. We evaluate three state-of-the-art LLMs (DeepSeek-V3, Claude Sonnet, GPT-4o) for code analysis, achieving up to 73.8% inter-model agreement on high-level features. This enables zero-shot prediction for unseen workloads with one-time extraction cost of \$0.018 per program.
4. The effectiveness of the models and few-shot model-based learning approach is evaluated through extensive experiments by verified OpenMP benchmarks (BOTS and PolybenchC) and multiple embedded processors including NVIDIA Jetson TX2, Jetson Orin NX, RubikPi, and Intel Core i7. To reduce the overhead of the models to be run on a single core, we provide comprehensive tuning in terms of accuracy and architectural exploration.
5. The proposed scheduler is compared to the state-of-the-art heuristic-based schedulers [7] and Linux governors [9]. Our model-based approach achieves 358ms inference latency for subsequent decisions. First decisions on new benchmarks require 3.5 to 8.0s including one-time LLM feature extraction. First-decision latency is 8,300\$ times\$ faster than table-based profiling, while achieving $7.09 \times$ better energy efficiency than the Linux ondemand governor. The proposed regression models for temperature sensors also outperform the state-of-the-art's maximum mean squared error (MSE) by a factor of over 6.

The paper is organized as follows: Section 2 surveys related work, Section 3 describes motivation, Section 4 presents the framework including LLM-based feature extraction, Section 5 evaluates performance including LLM feature analysis, and Section 6 concludes the paper. The appendix provides complete LLM implementation details.

2 Related Work

Low-energy scheduling for multi-core platforms based on DVFS has received significant attention [70, 67, 66, 79, 69, 29, 14, 77, 13, 40, 75, 55, 56, 50, 28, 27, 36, 37, 68, 2, 1, 35]. The survey in [70] classifies all the low-energy parallel scheduling into energy-efficient, energy-aware, and energy-conscious styles, each based on heuristic, meta-heuristic, integer programming, and machine learning algorithms. Among

these algorithms, only data-oriented machine learning, surveyed in [48], relies on historically collected data and addresses different application dynamics.

Due to the integration of DVFS in most commercial processors and their standard profiling and control, machine-learning algorithms are gaining significance in providing a dynamic environment [74, 31, 19, 80, 48, 54, 63, 73, 39, 53, 59, 62, 8]. The previous work [48] shows most of the machine learning algorithms for DVFS are based on model-free reinforcement learning, which implements a direct RL approach. None of this existing work addresses feature evaluation challenges or sample collection overhead.

Few-shot learning encompasses diverse techniques like transfer learning, model-based RL, inverse RL, imitation learning, and meta-learning, all applicable to DVFS due to its sampling demands [61, 33, 64, 43, 22, 17, 23, 16, 71, 17, 5, 65, 51, 60]. While inverse RL infers reward functions from expert demonstrations [44], model-agnostic meta-learning adapts to new tasks with minimal data [21], and model-based RL approximates transition functions [42]. The works in [38, 30, 78, 76] utilize MARL, meta-state, transfer learning, and temporal dependencies on DVFS. The Q-learning algorithm in [74] turned off and on the clock on idle cycles FPGA instead of DVFS used in [19]. None of these works address few shot learning and learning overhead in RL-based DVFS governors. The existing few-shot learning approaches also need an expert demonstration or cannot directly be applied in embedded systems.

Previous studies have investigated runtime sampling complexities in RL-based DVFS and proposed thermal predictive modeling for multi-core processors to predict thermal states [72, 10, 19, 25, 34, 41, 62]. The works in [38, 30] focus on temperature and utilization metrics and implement a command module on a separate neural network server. The predictive modeling in [41, 25] predicts the future thermal behavior of the multi-core processors given transient and ambient states. However, these RL training methods are computationally expensive on a single platform, and temperature models are inaccurate. This paper introduces computationally efficient and accurate modeling and a learning approach without requiring extra client-server interaction for frequency scaling.

2.1 LLM-Based Code Analysis for Performance Prediction

Recent advances in Large Language Models (LLMs) have demonstrated remarkable capabilities in understanding and reasoning about source code [15, 12]. Models such as GPT-4 [46], Claude [4], and DeepSeek-Coder [18] have been trained on extensive code corpora, enabling them to perform tasks ranging from code generation and bug detection to semantic analysis and performance optimization.

Several studies have explored using machine learning for static code analysis and performance prediction. Laaber et al. [32] demonstrated that benchmark stability can be predicted using 58 statically-computed source code features without execution. In the HPC domain, researchers have applied neural networks to OpenMP program analysis, including predicting optimal thread counts [52] and detecting data races using graph neural networks. Recent work by Nichols et al. [45] investigated whether LLMs can predict GPU kernel performance characteristics (compute-bound vs. memory-bound) using only source code, achieving up to 64% accuracy with reasoning-capable models in zero-shot settings.

However, existing approaches for DVFS and task scheduling typically rely on runtime profiling or benchmark-specific identifiers, limiting their applicability to new workloads. Traditional static analysis tools extract syntactic features (loop counts, pragma annotations) but cannot capture semantic properties such as algorithmic complexity or memory access patterns that require understanding code behavior. This work bridges this gap by employing LLMs to extract semantic features from OpenMP programs, enabling zero-shot performance prediction for unseen workloads without the extensive profiling overhead required by existing methods.

3 Background and Motivation

Online learning to adjust DVFS and task-to-core allocation with a small number of hardware samples is a practical approach to control heat generation and energy consumption in multi-core platforms.

3.1 Background

Here we give some background on DVFS, task-to-core allocation as optimization knobs, and the online learning based on RL for these two approaches.

DVFS. The power consumption and thermal condition of a processor are proportional to the voltage and frequency, which also determine the workload performance. In our case, performance is measured as the makespan, i.e., the time taken from the start to the completion of the workload. The workloads considered here are BOTS benchmarks such as Strassen, FFT, and others, parallelized through the OpenMP API [20]. Existing Linux governors and energy-aware DVFS heuristics use utilization metrics to determine workload demand and adjust voltage and frequency [9, 24, 38]. For instance, the ondemand governor increases the frequency instantly when utilization crosses a threshold; similarly, the conservative governor incrementally increases frequency after exceeding the utilization threshold. The schedutil governor uses predictive utilization over a specific time window to predict future workload demand [9]. These governors achieve sub-millisecond decision latency but lack workload-aware optimization.

Task-to-Core Allocation. Due to the different performance characteristics of different types of cores and non-uniform memory access (NUMA), i.e., performance is relative to the proximity to memory, the makespan and power/energy consumption differ with respect to different core allocations. For example, in the NVIDIA Jetson TX2, the ARM Cortex-A57 cores correspond to cores 2, 3, 4, and 5, which are power-efficient cores, while the NVIDIA Denver cores (cores 0 and 1) are more suited for performance-critical tasks and are by default turned off for power efficiency. It is possible to allocate a set of cores and memory nodes through the `cpuset` feature of the Linux kernel. Additionally, CPU affinity, i.e., binding specific threads of execution to specific cores, helps reduce context switches and enhances performance in terms of makespan and energy efficiency. Intelligent allocation of cores to the input workload helps distribute processing, reducing the concentration of processing in a specific spot in the processor, thereby decreasing the thermal throttling possibility.

Online Learning for DVFS and Task-to-Core Allocation. The online learning approach for DVFS and task-to-core allocation is often based on RL using a Markov Decision Process (MDP) that depends on the previous state (observed multi-core platform performance data), the taken action (frequency scaling and task-to-core allocation), and observing the current state after applying this action. The objective in RL is to apply actions based on observed states that maximize the expected sum of future rewards with the defined reward function [6, 26]. In a direct RL approach, the learning algorithm is based on exploration and exploitation; exploration involves taking random actions, and exploitation refers to taking actions based on the policies trained through observing the previous and current states. This training continues for a time horizon until the learning algorithm converges. For example, with Q-learning, the states mapped to the actions are given values called Q-values, and convergence happens when the taken actions are optimized according to the defined reward function in terms of maximum accumulated rewards. RL methods using neural networks typically achieve inference latencies of 1-10 milliseconds on embedded platforms.

Deep Q-learning and Enhanced D3QN. The profiling data extracted from parallel workloads (e.g., BOTS benchmarks) is continuous, meaning the state space cannot be simply mapped to the action space through a Q-function in Q-learning. Deep Q-learning, a sophisticated RL algorithm, leverages neural networks to approximate these Q-values. Deep Q-learning provides sample efficiency by training through past experiences stored as state-action pairs inside a replay buffer. To mitigate issues like overestimation of actions, the Q-function utilizes Dueling Deep Q-Networks (D3QN), i.e., decomposing the Q-function into a value function and an advantage function, where the value function gives a global value for each corresponding state and the advantage function evaluates the advantage of taking an action in the corresponding state. The Q-value is assigned to a corresponding state-action pair by taking an action based on the same deep Q-network with respect to the target, i.e., maximized future rewards. To make the action selection independent from the module that calculates the Q-value, a parallel Deep Q-network is designed, resulting in a double dueling deep Q-Network (D3QN). These strategies collectively allow the Deep Q-Network to accurately learn optimal configurations, such as adjusting CPU frequencies and

allocating tasks to specific cores. As a result, the system can dynamically manage multi-core resources, achieving improved performance and energy efficiency through a stable and data-driven policy.

Table-Based Heuristic Scheduling. State-of-the-art energy-aware schedulers such as the precise scheduler [7] achieve near-optimal energy efficiency through exhaustive offline profiling, generating lookup tables by executing tasks across all frequency-core combinations. However, table generation requires extensive offline profiling (hours to days), and any workload change necessitates complete regeneration. While table lookup achieves sub-millisecond latency, the lack of runtime adaptability limits deployment in dynamic environments.

3.2 Motivation on Model-Based MARL

Model-based RL provides a more efficient, adaptable, and robust framework for optimizing DVFS and task-to-core allocation in multi-core systems, achieving fast convergence and low decision latency.

3.3 Limitations of Utilization-Based DVFS

Most of the available Linux kernel governors take CPU utilization to scale voltage and frequency. Utilization is defined as:

$$\text{Utilization} = \frac{T_{\text{busy}}}{T_{\text{busy}} + T_{\text{idle}}}$$

Here, T_{busy} is the time the processor is active (including both execution and stall times), and T_{idle} is the idle time. The busy time T_{busy} comprises both *active* time (T_{active}), when the processor is executing instructions, and *stall* time (T_{stall}), when execution is delayed due to factors like branch mispredictions, context switching overhead, cache misses, etc. [24]. Stall time can account for more than 50% of a workload’s execution time [38], yet utilization-based DVFS does not differentiate between the active and stall times. Thus, the utilization-aware frequency scaling may result in a less effective solution to match the frequency to the actual demand of the workload.

3.4 Challenges in Task-to-Core Allocation

Due to the characteristics of different core types and different properties of tasks, the set and the number of cores to be allocated to the parallel workload should be carefully determined. Many modern processors support heterogeneous computing by combining cores with different characteristics to enhance power efficiency and performance capabilities. Moreover, many modern processors have non-uniform memory access (NUMA), i.e., cores have different proximity to memory locations, resulting in performance degradation for distant cores. Selecting the cores also affects thermal throttling; overloading nearby cores can stall workload execution and accelerate processor aging. Selection of the number of cores to be allocated to the parallel tasks is also important. For example, in an OpenMP workload, where each thread of execution represents a core, *tied* tasks should be restricted to execute on the allocated core. In contrast, *untied* tasks can migrate to other cores. Unpredictable execution time of a tied task, caused by branch misses, can lead to overall unpredictability in the workload’s makespan. This introduces timing unpredictability, impacting the overall makespan and energy/power consumption. As a result, increasing the number of allocated cores in this case increases unpredictability and does not lead to improved performance [3]. In sum, to make informed decisions on task-to-core allocation, observation variables such as branch misses, cache misses, context switches, and each core’s temperature should be given appropriate attention.

Figure 1 highlights the changes of observation features at different frequency levels and sets of cores used for estimating the important performance metrics such as energy consumption and efficient voltage and frequency scaling and core allocation. The data is extracted from performance monitoring on an NVIDIA Jetson TX2 with 6 cores that runs the FFT benchmark parallelized through the OpenMP API. The frequency is split into 12 levels, level 0 representing the lowest frequency and level 11 representing the highest frequency. Core 0 is not allocated to the benchmark to retain system interrupt handler

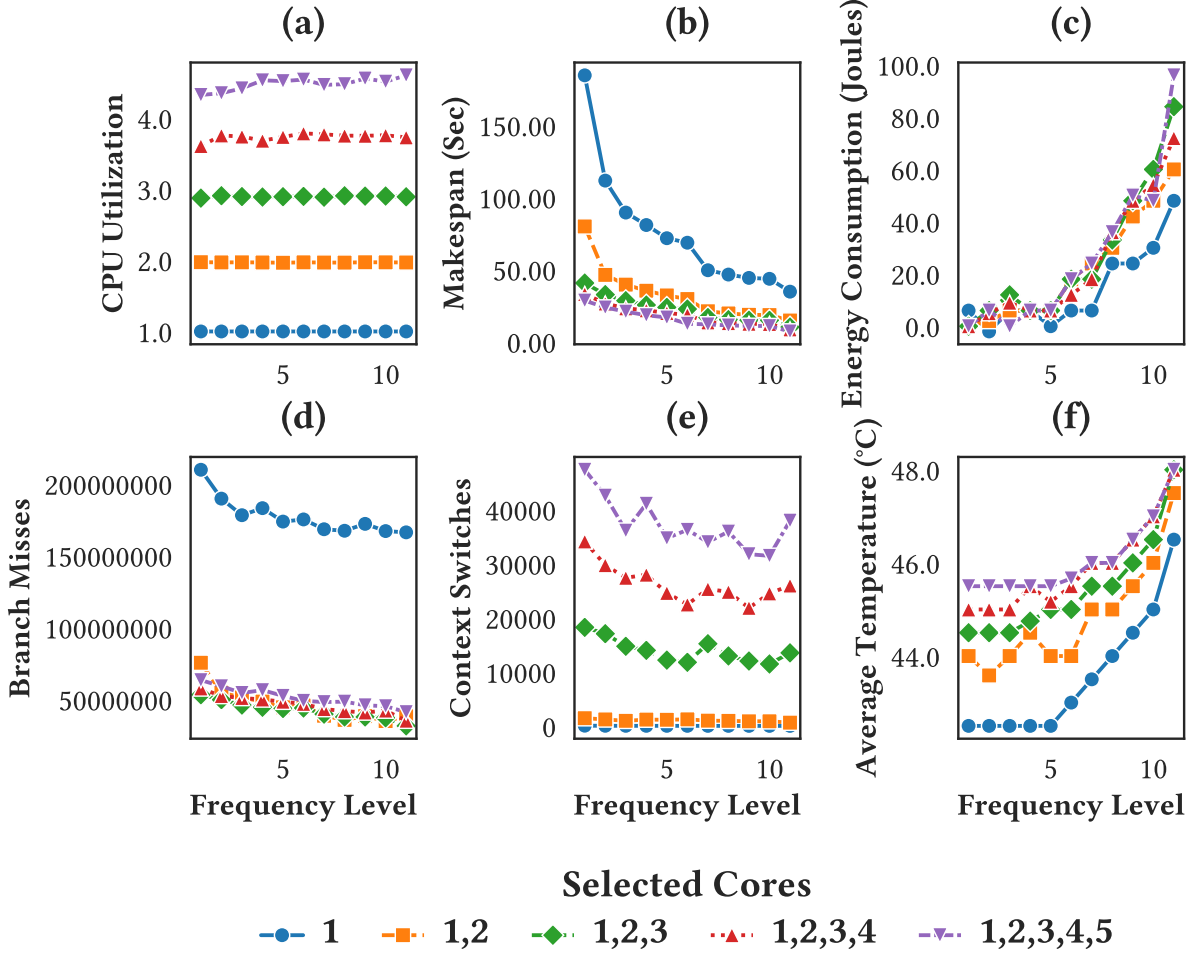


Figure 1: Performance metrics (CPU utilization, makespan, energy consumption, branch misses, context switches, and average temperature) for NVIDIA Jetson TX2 running the FFT benchmark parallelized through OpenMP API. Results highlight different responses of performance metrics to changes in different frequencies and selected cores.

performance, which is mostly done at core 0. The results depict six important metrics across frequency levels and core allocation configurations. CPU utilization (Figure 1(a)) increases with more cores and shows minimal impact from frequency scaling. Makespan (Figure 1(b)) reduces with higher frequency but shows diminishing returns when cores are more than two. Energy consumption (Figure 1(c)) increases sharply with higher frequency and core count, reducing efficiency. There is a big gap in branch misses when moving from one core to multiple cores, but it is largely unaffected by frequency (Figure 1(d)). Context switches rise with more cores, indicating inefficiency in core usage (Figure 1(e)). Average temperature increases with frequency and core count, risking thermal throttling (Figure 1(f)).

3.5 The Need for Environment Modeling and Multi-Agent RL

To effectively address both DVFS and task-to-core allocation while enhancing sample efficiency, it is crucial to develop an accurate environment model and employ a multi-agent reinforcement learning (RL) framework. An accurate environment model captures the system's characteristics, including hardware architecture, workload behavior, and their interactions, enabling low-cost synthetic sample generation for *few-shot* learning. By modeling the environment and incorporating factors such as branch misses, cache misses, and context switches, more precise and efficient strategies for energy optimization can be devised.

Implementing a multi-agent RL approach allows multiple agents to focus on different optimization tasks, such as frequency scaling and core allocation, each with potentially different reward definitions tailored to their specific goals. This specialization enhances the generalizability and effectiveness of the

online learning process, as agents can learn optimal strategies in parallel and adapt to changing conditions more quickly. Together, environment modeling and multi-agent RL provide a robust framework for dynamically managing multi-core resources, leading to improved performance and energy efficiency. Model-based MARL addresses the trade-off between decision quality and decision latency: while table-based methods achieve optimal energy efficiency, their offline profiling requires hours. In contrast, model-based RL achieves $20\times$ faster convergence with inference latencies under 10ms, which is orders of magnitude faster than table regeneration, enabling practical deployment with energy accuracy within 4% of optimal.

3.6 LLM-Based Code Analysis for Workload Profiling

Limitations of Traditional Static Analysis. Traditional approaches to workload characterization for DVFS and task scheduling rely on either runtime profiling or syntactic static analysis. Runtime profiling requires executing programs across all hardware configurations. This process takes hours to days for comprehensive coverage and must be repeated for each new workload or platform. Syntactic static analysis tools such as Tree-sitter and compiler front-ends can extract structural features (loop counts, pragma annotations, variable declarations), but they fundamentally lack the ability to understand the *semantic* meaning of code. For instance, a traditional parser can count the number of loops but cannot determine whether those loops exhibit strided memory access patterns, have data dependencies that limit parallelization, or are amenable to vectorization. This limitation is particularly problematic for performance prediction because execution time depends heavily on algorithmic complexity, memory access locality, and parallelization overhead. These are properties that require understanding what the code *does*, not merely how it is structured.

The Generalization Problem. A critical limitation of existing performance prediction approaches is their reliance on benchmark identifiers or application-specific lookup tables. Models trained with benchmark IDs can achieve high accuracy on known programs but cannot generalize to *new, unseen programs*. When a novel workload is introduced, the entire profiling process must be repeated, negating the benefits of learned models. This lack of generalization capability severely limits practical deployment, especially in dynamic embedded environments where workloads change frequently.

LLM-Based Semantic Code Understanding. Recent advances in Large Language Models (LLMs) have demonstrated remarkable capabilities in understanding source code at a semantic level [15]. Models such as GPT-4 [46], Claude [4], and DeepSeek-Coder [18] have been trained on vast corpora of code and natural language, enabling them to reason about algorithmic complexity, identify parallelization patterns, and assess memory access characteristics. Unlike traditional static analysis, LLMs can understand the *intent* behind code constructs and make informed judgments about performance-relevant properties. For example, an LLM can recognize that nested loops over matrix indices with specific access patterns indicate matrix multiplication with spatial locality along rows but poor locality along columns. Such insights would require sophisticated, manually-crafted analysis rules to extract traditionally.

Zero-Shot Feature Extraction for Unseen Programs. The key advantage of LLM-based feature extraction is enabling *zero-shot* performance prediction for programs not seen during training. By replacing benchmark-specific identifiers with semantic features (algorithmic complexity, memory access patterns, parallelization characteristics), a prediction model can generalize to entirely new programs. When a new workload is introduced, the LLM extracts its semantic features without any execution, and the trained model predicts performance based on these features. Recent work has demonstrated this capability: researchers have shown that LLMs can predict GPU kernel performance characteristics using only source code and hardware specifications, eliminating the need for execution-time profiling [45]. Similarly, studies on predicting code coverage without execution [58] and using neural networks to classify OpenMP program behavior [52] highlight the growing feasibility of execution-free code analysis.

Complementing Hardware Profiling with Semantic Features. While hardware performance counters (cache misses, branch mispredictions, context switches) provide valuable runtime information, they cannot be obtained without execution and are inherently tied to specific hardware configurations.

LLM-extracted semantic features complement hardware profiling by providing platform-agnostic characterization: algorithmic complexity remains $O(n \log n)$ regardless of whether the code runs on ARM or x86; memory access patterns are determined by the algorithm, not the cache hierarchy. This separation enables transfer learning, where models trained on one platform can leverage semantic features to adapt to new platforms with minimal recalibration. In this work, we evaluate three state-of-the-art LLMs (DeepSeek-V3, Claude Sonnet, and GPT-4o) for extracting 13 semantic features from OpenMP parallel programs, demonstrating how these features enable zero-shot prediction for unseen workloads.

4 Design of Model-Based Thermal- and Energy-Aware MARL

The proposed framework enables few-shot learning by generating synthetic data for agents that manage frequency scaling and task-to-core allocation on multi-core platforms, achieving low decision latency and fast convergence compared to exhaustive table-based approaches.

4.1 Design of MARL

Optimizing both DVFS and task-to-core allocation through RL is impractical due to high-dimensional action space and we need to break actions through introduction of multiple agents with separate goal definitions, which also reduces inference latency by decomposing complex decisions.

High-Dimension Action Space. The goal of the thermal- and energy-aware parallel scheduling in this paper is to dynamically adjust the voltage and frequency of the subset of the high priority cores based on cores and parallel workload characteristics. Regarding a naive single-agent implementation, the action space for this environment would be exponentially related to the frequency levels, the number of cores, and the combination of cores altogether, as shown in the following observation.

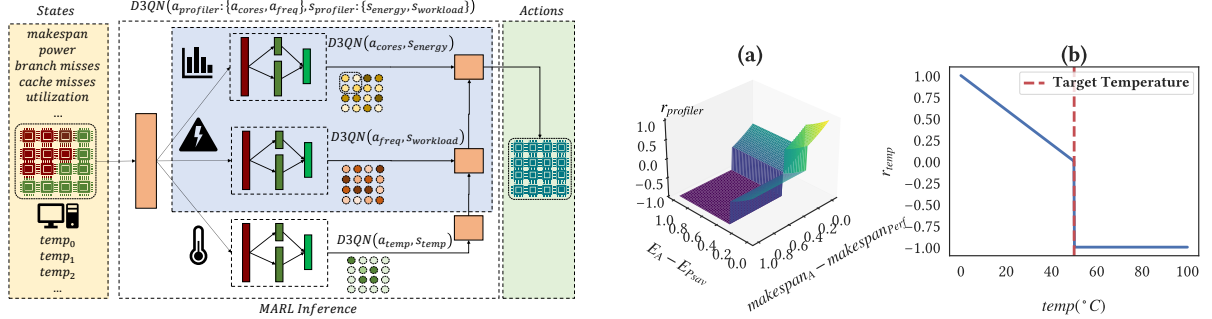
Observation: Consider a multi-core platform environment with m cores with adjustable per-core frequencies in the range of n frequencies; the number of actions to select some combinations of l cores with pre-tuned frequencies would be upperbounded by m^n .

To construct the action space, l cores must be selected from a total of m cores, which can be achieved using a combination formula like $\binom{m}{l}$. Suppose we only assign one frequency to all cores in the combination of cores in the range of n frequency conditions. In that case, the number of possible actions can be obtained by summing over the different numbers of core choices using a binomial coefficient. Thus, the total number of actions, disregarding frequency, is given by $\sum_{i=1}^m \binom{m}{i}$, which can be approximated to 2^m actions. However, suppose we include each core in the selected combination of cores to be associated with a frequency in the range of n frequencies; the previous formula changes to $\sum_{i=1}^m \binom{m}{i} 2^n$ that can be upper-bounded by m^n . For table-based approaches like the precise scheduler [7], this exponential action space necessitates exhaustive offline profiling across all configurations, requiring hours to days of execution time.

To address this challenge, we adopt a collaborative hierarchical MARL approach, as shown in Figure 2a. This approach decomposes the problem into lower-dimensional sub-problems handled by separate agents implemented as D3QN. The final action is a combination of each agent's decision. We use two primary agents:

- *Profiler Agent*: Assesses workload performance to minimize energy consumption and makespan by determining the appropriate number of cores and the operating frequency
- *Temperature Agent*: Prioritizes cores based on their temperature to prevent heat concentration.

According to Figure 2a, the action that assigns frequency to a core is called (a_{freq}) and the input energy consumption state (s_{energy}) determines Q-value $Q(a_{freq}, s_{energy})$, while the action that assigns the number of cores is called (a_{cores}) based on workload performance state $(s_{workload})$ that determines Q-value $Q(a_{cores}, s_{workload})$. To decrease the computational overhead, these two agents are combined resulting in profiler action $a_{profiler} : \{a_{cores}, a_{freq}\}$ from the profiler state $s_{profiler} : \{s_{energy}, s_{workload}\}$.



(a) Hierarchical MARL Action Selection with Two Agents: The Profiler Agent determines the number of active cores and the operating frequency based on performance and energy consumption states. The Temperature Agent assigns priority levels to cores based on temperature states. The combined actions result in prioritized cores and the appropriate number allocated to tasks, reducing computational complexity and decision latency.

(b) Reward function definitions for (a) the Profiler Agent and (b) the Temperature Agent. (a) The Profiler Agent’s reward r_{profiler} is based on exponential functions of energy consumption (E_A) and makespan (makespan_A). Here, a threshold factor ($c_{\text{th}} = 0.3$) and a steepness factor ($c_{\text{st}} = 0.5$) determine the reward focus. (b) The Temperature Agent’s reward r_{temp} changes linearly based on core temperature (temp_i), aiming to maintain temperatures below the threshold of 50°C.

Figure 2: MARL design: (a) Hierarchical action selection architecture and (b) reward function definitions.

Priority assignment action (a_{temp}) is based on the core thermal state (s_{temp}), determining Q-value $Q(a_{\text{temp}}, s_{\text{temp}})$. Assigning a frequency from n frequency levels to m cores results in $m \times n$ possible actions. Selecting from m possible number of cores results in m choices, and for priority selection, we have choices from $m \times m$ possible actions. Introducing sequential action selection in MARL reduces this to $m \times m + m \times n + m$ possible choices, enabling inference latency under 10ms on embedded platforms.

Reward Function Definition. The reward functions for the Profiler and Temperature agents are designed to guide the system toward optimal performance and energy efficiency. Unlike previous studies [38, 30], which rely on CPU utilization and frame rate as target metrics, our approach focuses on makespan and energy consumption of suboptimal conditions defined by performance and powersave linux governors to provide a more accurate assessment of workload performance. This shift addresses the limitations of utilization metrics, which can be misleading by overlooking stall times. Additionally, to prevent thermal throttling, we enforce a temperature limit of 50°C based on the thermal throttling threshold of the Jetson TX2.

For the Temperature agent, we employ a linear reward function designed to maintain core temperatures below the 50°C threshold. Specifically, for each core, if its temperature exceeds 50°C, the reward is set to -1 , penalizing actions that lead to overheating. Conversely, if the temperature remains below the threshold, the reward is calculated as the difference between 50°C and the current temperature of the core. Mathematically, the reward for core i is defined as:

$$r_{\text{temp}}^i = \begin{cases} -1 & \text{if } \text{temp}_i > 50^\circ\text{C}, \\ 50 - \text{temp}_i & \text{otherwise.} \end{cases}$$

The overall temperature reward is then computed as the average of these individual rewards across all m cores:

$$r_{\text{temp}} = \frac{1}{m} \sum_{i=1}^m r_{\text{temp}}^i.$$

This structure incentivizes the agent to keep all cores cool, thereby preventing thermal throttling and ensuring sustained performance.

In contrast, the Profiler agent utilizes an exponential reward function to balance energy consumption and makespan. The reward is determined based on how closely the system’s performance metrics approach their target values. We define two parameters: the *threshold factor* $c_{\text{th}} = 0.3$ controls the

penalization boundary relative to baseline performance, and the *steepness factor* $c_{st} = 0.5$ controls how rapidly rewards decay as metrics deviate from targets. Specifically, if the agent total energy consumption (E_A) exceeds the target set by the powersave governor (E_{Psav}) or if the agent makespan (makespan_A) surpasses the target set by the performance governor ($\text{makespan}_{\text{perf}}$) by a factor of c_{th} , the reward is set to -1 , discouraging inefficient configurations. Otherwise, the reward increases exponentially as energy consumption and makespan approach their targets, defined as:

$$r_{\text{energy}} = e^{-c_{st} \times \frac{E_A - E_{Psav}}{c_{th}}} \times 2 - 1,$$

$$r_{\text{makespan}} = e^{-c_{st} \times \frac{\text{makespan}_A - \text{makespan}_{\text{perf}}}{c_{th}}} \times 2 - 1.$$

The final profiler reward is the average of the energy consumption and makespan rewards:

$$r_{\text{profiler}} = \frac{r_{\text{energy}} + r_{\text{makespan}}}{2}.$$

Here, E_{total} represents the total energy consumption, and makespan denotes the workload completion time. The parameters c_{th} and c_{st} control the threshold for penalization and the steepness of the exponential increase, respectively. By adjusting these parameters, we can prioritize either energy efficiency or makespan based on the specific optimization objectives in each agent.

Figure 2b illustrates these two distinct reward functions, showing how the profiler agent optimizes for energy and makespan while the temperature agent maintains thermal constraints.

Complexity Analysis of Agents. Each agent in the proposed energy-aware hierarchical MARL scheduler requires individual training to assign meaningful weights to observations for reward evaluation, increasing computational complexity. However, this complexity is justified by the improved sample efficiency achieved through the off-policy Q-learning method. We employ the D3QN to address this, which provides practical agent training. Once trained, neural network inference is fast (sub-10ms), enabling practical deployment. In case of model inference failure or anomalous predictions, the system gracefully degrades to the Linux ondemand governor, which represents our baseline and ensures continued operation without service interruption.

Let N_{agent} represent the number of agents, N_{hidden} be the number of hidden layer neurons, N_{state} be the dimension of the input observations, and N_{actions} be the dimension of the output actions. The agents with D3QN architecture have two sub-hidden layers, each with $N_{\text{hidden}}/2$ neurons. The first layer calculates advantages, resulting in an output layer of size equal to the number of actions N_{actions} . The second layer calculates values and has a single neuron in its output layer.

The total number of network parameters for a single agent is:

$$\begin{aligned} \text{Parameters} = 2 \times & ((N_{\text{state}} \times N_{\text{hidden}} + N_{\text{hidden}}) \\ & + (N_{\text{hidden}} \times N_{\text{actions}} + N_{\text{actions}}) \\ & + (N_{\text{hidden}} \times 1 + 1)) \end{aligned}$$

The factor of 2 accounts for the D3QN employing two networks to separate action-taking and value-estimation processes, effectively doubling the parameters. Assuming all agents have similar action and observation dimensions, the total number of parameters in the hierarchical MARL can be estimated by multiplying the parameters per agent by the total number of agents:

$$\text{Total Parameters} = N_{\text{agent}} \times \text{Parameters}$$

To enhance the model's efficiency regarding computational complexity, it is essential to optimize the number of hidden neurons N_{hidden} and carefully balance the number of agents N_{agent} . Techniques such as parameter sharing among agents, pruning less significant neurons, and employing more efficient network architectures can significantly reduce the total number of parameters. Additionally, leveraging hardware accelerations like GPUs or specialized AI processors can mitigate the computational overhead, ensuring

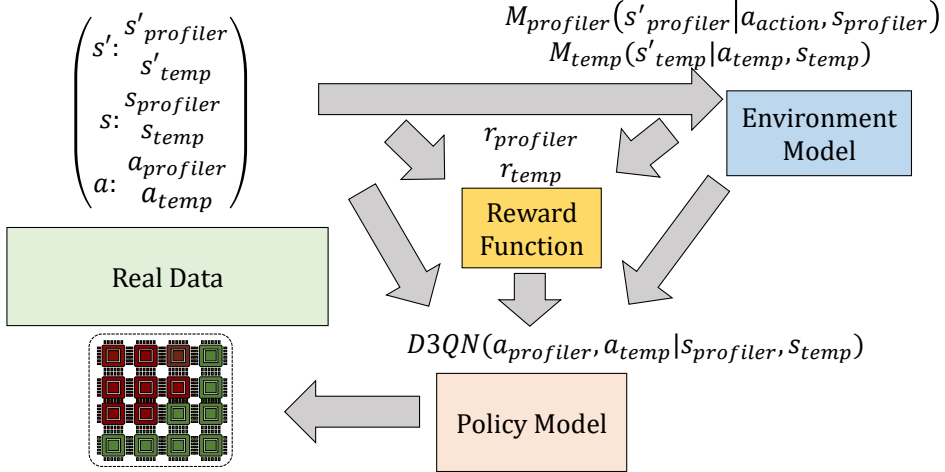


Figure 3: The simplified design of model-based RL for temperature- and energy-aware core allocation for multi-core processors.

scalable and efficient training of the hierarchical MARL system. In this implementation, we separate the client that is the targeted Jetson TX2 as platform from the server where the online learning algorithm is implemented to deal with computational complexity. This client-server architecture amortizes training cost offline while maintaining lightweight inference on the embedded platform, achieving decision latency orders of magnitude faster than table regeneration for any configuration changes.

4.2 Environment Design and Modeling

The model of the environment consists of a model for temperature agent and a model for profiler agent implemented and verified through a variety of regression algorithms, selected for both accuracy and low inference latency.

Proposed Model-Based Hierarchical MARL Approach. In a model-free RL context, agents interact directly with the environment and train based on the real data. In contrast, model-based RL involves simulation data along with the real data extracted from the environment. Inference from the dynamic model (planning) speeds up agent training and hyperparameter tuning, requiring fewer samples for convergence than only gathering real data. As shown in Figure 3, agents are trained either with environment observations or the dynamic model. This model-based approach achieves significantly faster convergence compared to model-free methods and avoids the extensive offline profiling required by table-based approaches.

The proposed model-based hierarchical MARL approach is inspired by the Dyna-Q algorithm [49], as shown in Algorithm 1. Dyna-Q is particularly well-suited for this application because it effectively integrates learning and planning, allowing agents to leverage both real and simulated experiences. This integration enhances sample efficiency, which is crucial in complex multi-agent environments like energy-aware scheduling in multi-core processors where real-world interactions can be time-consuming and resource-intensive. By utilizing a dynamic model to generate simulated experiences, the approach accelerates training convergence and reduces the reliance on extensive real-world data collection. Additionally, Dyna-Q's framework supports scalability and robustness, enabling the system to adapt to varying workload patterns and efficiently manage multiple agents operating at different levels of abstraction. Compared to exhaustive table generation, this approach completes training in minutes rather than hours while enabling runtime adaptation.

The Algorithm 1 begins by initializing separate replay memories for both the profiler and temperature

agents, along with their respective dynamic models and value functions. Parameters such as threshold ζ for planning steps and batch size β for training are also set. The training process is divided into multiple episodes, each starting with the initialization of the profiler and temperature states. Within each episode, the algorithm enters a loop that continues until a termination condition is met for either agent. In the **Direct RL** phase, each agent selects an action based on its current policy derived from its respective Q-value function ($D3QN_{\text{profiler}}$ and $D3QN_{\text{temp}}$), executes the action in the environment, and observes the resulting next state, reward, and done flag. These transitions are stored in their corresponding real replay memories (B_{profiler} and B_{temp}). If the conditions for training the dynamic models are satisfied, only the profiler's model M_{profiler} is trained using samples from B_{profiler} . The temperature agent does not have a separate dynamic model.

Following the **Planning** phase, the algorithm generates a predefined number of simulated transitions (ζ steps) for each agent. These simulated transitions are generated using the profiler's dynamic model M_{profiler} , and the thermal synthetic data is derived from the profiler's predictions. For each planning step, actions are generated (either randomly or based on the current policy), and the dynamic models predict the subsequent states and rewards. These simulated transitions are stored in the simulated replay memories (B'_{profiler} and B'_{temp}). The profiler's simulated transitions are stored in B'_{profiler} , while the thermal synthetic transitions are inferred and stored in B'_{temp} based on the profiler's predictions. If the conditions to train the agents are met, minibatches are sampled from both the real and simulated replay memories, and the Q-value functions ($D3QN_{\text{profiler}}$ and $D3QN_{\text{temp}}$) are trained using these samples. The current states are then updated to the next states, and the loop checks whether the episode should terminate based on the done flags. This iterative process ensures that both agents benefit from real and simulated experiences, enhancing their learning efficiency and adaptability in managing energy consumption and thermal states within multi-core processors.

By adopting the Dyna-Q-inspired framework, the proposed hierarchical MARL approach achieves a balance between efficient learning and practical scalability. This ensures that the system can effectively manage energy consumption and thermal states in multi-core processors while maintaining computational efficiency and adaptability to dynamic workloads. Optimizing the training conditions and leveraging both real and simulated data streams allows the model to converge faster and operate reliably in complex, real-world scenarios.

Different Environment Models and their Computational Complexity. To determine the most efficient architecture for the environment model, this study evaluates several state-of-the-art regression models in predicting profiler states (s'_{profiler}) and temperature states (s'_{temp}). The models are trained using data that includes profiler state information (s_{profiler}), temperature state (s_{temp}), and their corresponding actions (a_{profiler} for the profiler model and a_{temp} for the temperature model). The regression models considered are Simple Fully Connected Networks (FCNs), Convolutional Neural Networks (CNNs), Recurrent Neural Networks (RNNs), Long Short-Term Memory Networks (LSTMs), and Attention-Based Networks. Model selection prioritizes both prediction accuracy and inference latency to enable efficient planning.

A Simple Fully Connected Network with one hidden layer consists of an input layer of size N_{input} , where $N_{\text{input}} = N_{\text{state}} + N_{\text{action}}$. The hidden layer contains N_{hidden} neurons, and the output layer has N'_{state} neurons corresponding to the predicted next profiler state. The total number of trainable parameters in an FCN is calculated as:

$$\begin{aligned} \text{Parameters}_{\text{FCN}} = & N_{\text{input}} \times N_{\text{hidden}} \\ & + N_{\text{hidden}} \times N'_{\text{state}} \\ & + N_{\text{hidden}} + N'_{\text{state}} \end{aligned}$$

FCN models achieve inference latencies of 2-5ms on embedded platforms.

Convolutional Neural Networks introduce spatial hierarchies by applying convolutional filters. For a one-dimensional convolutional layer with a kernel size of K , C_{out} output channels, and input dimension

Algorithm 1 Model-Based Hierarchical Multi-Agent RL

```

1: Initialize:
2:   Replay memories  $B_{\text{profiler}}$  and  $B'_{\text{profiler}}$  for the profiler agent
3:   Replay memories  $B_{\text{temp}}$  and  $B'_{\text{temp}}$  for the thermal agent
4:   Dynamic model  $M_{\text{profiler}}$  for the profiler agent
5:   Value functions  $D3QN_{\text{profiler}}$  and  $D3QN_{\text{temp}}$ 
6:   Parameters: planning threshold  $\zeta$ , batch size  $\beta$ 
7: for each episode = 1 to  $H$  do
8:   Initialize states  $s_{\text{profiler}}$  and  $s_{\text{temp}}$ 
9:   while not done do
10:    Direct RL:
11:      Select action  $a_{\text{profiler}}$  using  $D3QN_{\text{profiler}}$ 
12:      Select action  $a_{\text{temp}}$  using  $D3QN_{\text{temp}}$ 
13:      Execute actions  $a_{\text{profiler}}$  and  $a_{\text{temp}}$  in the environment
14:      Observe next states  $s'_{\text{profiler}}$ ,  $s'_{\text{temp}}$ 
15:      Observe rewards  $r_{\text{profiler}}$ ,  $r_{\text{temp}}$ , and done flags  $d_{\text{profiler}}$ ,  $d_{\text{temp}}$ 
16:      Store  $(s_{\text{profiler}}, a_{\text{profiler}}, r_{\text{profiler}}, s'_{\text{profiler}})$  in  $B_{\text{profiler}}$ 
17:      Store  $(s_{\text{temp}}, a_{\text{temp}}, r_{\text{temp}}, s'_{\text{temp}})$  in  $B_{\text{temp}}$ 
18:      if Model training condition is met then
19:        Train  $M_{\text{profiler}}$  using samples from  $B_{\text{profiler}}$ 
20:      end if
21:      Planning:
22:      for each planning step = 1 to  $\zeta$  do
23:        Generate action  $a'_{\text{profiler}}$  (randomly or from policy)
24:        Predict  $s''_{\text{profiler}}$ ,  $r''_{\text{profiler}}$  using  $M_{\text{profiler}}$ 
25:        Derive  $s''_{\text{temp}}$ ,  $r''_{\text{temp}}$  from  $s''_{\text{profiler}}$ 
26:        Store  $(s_{\text{profiler}}, a'_{\text{profiler}}, r'_{\text{profiler}}, s''_{\text{profiler}})$  in  $B'_{\text{profiler}}$ 
27:        Store  $(s_{\text{temp}}, a_{\text{temp}}, r'_{\text{temp}}, s''_{\text{temp}})$  in  $B'_{\text{temp}}$ 
28:      end for
29:      if Agent training condition is met then
30:        Sample minibatch from  $B_{\text{profiler}}$  and  $B'_{\text{profiler}}$ 
31:        Train  $D3QN_{\text{profiler}}$  with the minibatch
32:        Sample minibatch from  $B_{\text{temp}}$  and  $B'_{\text{temp}}$ 
33:        Train  $D3QN_{\text{temp}}$  with the minibatch
34:      end if
35:      Update  $s_{\text{profiler}} \leftarrow s'_{\text{profiler}}$ ,  $s_{\text{temp}} \leftarrow s'_{\text{temp}}$ 
36:      Check termination: If  $d_{\text{profiler}}$  or  $d_{\text{temp}}$  is True, exit loop
37:    end while
38: end for

```

N_{input} , the number of trainable parameters is:

$$\begin{aligned} \text{Parameters}_{\text{CNN}} = & K \times N_{\text{input}} \times C_{\text{out}} \\ & + C_{\text{out}} \end{aligned}$$

CNN inference latency ranges from 4-8ms.

Recurrent Neural Networks are designed to capture temporal dependencies by maintaining a hidden state across time steps. For an RNN with N_{hidden} neurons, the number of parameters is:

$$\begin{aligned} \text{Parameters}_{\text{RNN}} = & N_{\text{input}} \times N_{\text{hidden}} \\ & + N_{\text{hidden}} \times N_{\text{hidden}} \\ & + N_{\text{hidden}} + N_{\text{hidden}} \times N'_{\text{state}} \\ & + N'_{\text{state}} \end{aligned}$$

Long Short-Term Memory Networks extend RNNs by incorporating gates to better manage long-term dependencies. An LSTM with N_{hidden} neurons has approximately three times the number of parameters compared to a standard RNN due to the additional forget, input, and output gates, resulting in higher inference latency.

Attention-Based Networks, inspired by Vaswani et al. [60], allow the model to focus on relevant parts of the input sequence simultaneously. In this work, a self-attention mechanism is coupled with a feedforward network. Let H denote the number of attention heads and N_{hidden} represent the hidden

dimension per head. Each attention head processes queries Q , keys K , and values V with dimension N_{hidden} . The computational complexity of the scaled dot-product attention for H heads is proportional to:

$$O((N_{\text{input}} + 2)^2 \times H \times N_{\text{hidden}} + (N_{\text{hidden}} + 1) \times N_{\text{input}})$$

Attention mechanisms exhibit higher inference latency but provide superior prediction accuracy.

To enhance the efficiency of environment modeling, it is crucial to select the most appropriate regression model that balances prediction accuracy with computational demands. Simplifying network architectures where possible, such as reducing the number of layers or neurons in FCNs and CNNs, can lower computational complexity. Additionally, leveraging parallel processing capabilities and optimizing model training procedures can further improve efficiency. Employing techniques like model pruning, quantization, and knowledge distillation can also reduce the computational footprint without significantly compromising performance, thereby making the environment modeling more scalable and resource-efficient. In practice, FCN and Conv1D architectures achieve over $6\times$ better temperature prediction accuracy than prior work while maintaining inference latencies under 5ms, enabling efficient planning with synthetic data generation.

4.3 Cross-Platform Model Transfer and Adaptation

A key advantage of our learned environment model is its ability to transfer across platforms without requiring exhaustive re-profiling. Unlike table-based approaches that must regenerate all lookup entries when deployed on new hardware, our neural network models encode generalizable relationships between workload characteristics, system configuration, and performance outcomes. This section describes our transfer learning methodology for cross-platform deployment.

4.3.1 Transfer Learning Methodology

We employ a two-stage transfer learning approach:

Stage 1: Zero-Shot Transfer. The environment model trained on the source platform (Jetson TX2) is directly applied to the target platform without any modification. This provides a baseline for transfer quality and works because workload characteristics, including algorithmic complexity, memory access patterns, and parallelism, are ISA-agnostic. Furthermore, relative performance trends such as frequency scaling impact and core allocation effects generalize across platforms, while neural network representations capture underlying physical relationships that remain consistent across hardware implementations.

Stage 2: Few-Shot Fine-Tuning. The transferred model is refined using a small number of samples (5, 10, or 50) collected from the target platform. This fine-tuning process adapts frequency scaling coefficients to platform-specific P-states, calibrates thermal prediction to accommodate different cooling solutions, and adjusts energy consumption estimates to match platform TDP characteristics.

4.3.2 Feature Classification for Transfer

We categorize features based on their transferability:

Platform-Agnostic Features (high transferability): These features exhibit strong generalization across different hardware architectures. They include algorithmic complexity and computational patterns, memory access locality and data structure characteristics, parallelism structure and task dependencies, as well as branch prediction patterns and control flow complexity.

Platform-Specific Features (require adaptation): These features require calibration when transferring between platforms. They encompass absolute frequency values (normalized to [0,1] range), per-core temperature readings (normalized to thermal headroom), energy consumption (normalized to platform TDP), and core count and heterogeneity configuration.

By normalizing platform-specific features relative to each platform’s operating range, we maximize the transferable knowledge while enabling platform-specific calibration through fine-tuning.

4.3.3 Transfer Learning Results

The cross-platform transfer learning results are presented in Section 5 (Table 5). Our experiments evaluate zero-shot transfer from Jetson TX2 to Orin NX and RubikPi platforms, demonstrating the domain shift effects when deploying learned models across different embedded architectures. The source platform achieves 10.9% MAPE (Mean Absolute Percentage Error), while zero-shot transfer shows 64.5% and 73.2% MAPE for Orin NX and RubikPi respectively, reflecting significant architectural differences between platforms.

4.3.4 Comparison with Table-Based Approaches

The transfer learning capability provides a fundamental advantage over table-based schedulers. While deploying a table-based scheduler on a new platform requires $T_{table} = m \times k \times |\Gamma| \times \rho \times \bar{t}$ profiling time, where m is the number of cores, k is the number of frequency levels, $|\Gamma|$ is the cardinality of the task set, ρ is the number of repetitions, and \bar{t} is the average execution time (typically 8 to 12 hours), our approach achieves 5.7ms RL inference latency, representing over 5 million times faster adaptation capability for practical deployment in heterogeneous fleet environments.

4.4 LLM-Based Semantic Feature Extraction

Traditional performance prediction models for DVFS scheduling rely on benchmark identifiers to distinguish workloads, creating a fundamental limitation: they cannot generalize to programs absent from the training set. When a new application arrives, exhaustive profiling across all frequency-core configurations must be repeated. This process requires 8 to 12 hours per program on our target platforms, where each benchmark execution takes 1 to 5 seconds. We address this limitation by replacing opaque benchmark identifiers with interpretable semantic features extracted directly from source code, enabling zero-shot prediction for previously unseen workloads.

4.4.1 Motivation: From Syntax to Semantics

The challenge of workload characterization without execution traces requires distinguishing between what code *contains* versus how it *behaves*. Traditional static analysis tools such as Tree-sitter [57] and compiler front-ends excel at extracting syntactic properties, such as counting loops, identifying OpenMP pragmas, and measuring code complexity metrics. However, these tools fundamentally cannot infer semantic properties that determine runtime behavior.

Consider the limitations of purely syntactic analysis. A parser detecting three nested loops cannot determine whether they implement $O(n^3)$ matrix multiplication or $O(n^{2.807})$ Strassen’s algorithm; the syntactic structure appears identical despite dramatically different scaling behavior. Similarly, array indexing syntax $A[i][j]$ reveals nothing about whether memory accesses exhibit unit-stride patterns amenable to hardware prefetching or scattered patterns that thrash the cache hierarchy. These semantic judgments require understanding algorithmic intent rather than merely parsing code structure.

Large language models trained on extensive code corpora offer a compelling solution. Unlike rule-based analyzers, LLMs can recognize algorithmic patterns, reason about data flow dependencies, and assess parallelization characteristics through learned representations of programming concepts. We leverage this capability to extract 13 semantic features that complement the 17 syntactic features obtained through traditional static analysis.

4.4.2 Two-Stage Feature Extraction Pipeline

Our feature extraction operates in two complementary stages. The first stage employs Tree-sitter to extract syntactic features capturing the structural composition of OpenMP programs: control flow metrics such as loop depth and nesting complexity, OpenMP directive counts including parallel regions and task constructs, synchronization primitives such as critical sections and atomic operations, and variable

Table 1: Inter-Model Agreement Rates for Semantic Features (%)

Feature	DS-CL ^a	DS-GPT ^b	CL-GPT ^c	All 3
dominant_operation	83.3	88.1	76.2	73.8
algorithmic_complexity	69.0	78.6	66.7	59.5
temporal_locality	66.7	81.0	47.6	47.6
load_balance	40.5	88.1	47.6	38.1
parallelization_overhead	45.2	59.5	64.3	38.1
vectorization_potential	47.6	69.0	50.0	35.7
spatial_locality	59.5	52.4	50.0	31.0
memory_access_pattern	61.9	33.3	28.6	21.4
data_dependency_type	38.1	42.9	50.0	21.4
cache_behavior_pattern	69.0	33.3	28.6	16.7
false_sharing_risk	23.8	50.0	40.5	14.3

^a DS-CL: DeepSeek-V3 vs. Claude Sonnet agreement.

^b DS-GPT: DeepSeek-V3 vs. GPT-4o agreement.

^c CL-GPT: Claude Sonnet vs. GPT-4o agreement.

scope classifications distinguishing shared, private, and reduction variables. These 17 features provide a syntactic fingerprint of code structure but cannot distinguish semantically different algorithms with similar structural properties.

The second stage queries large language models to extract semantic features requiring deeper code understanding. We employ three state-of-the-art models, namely DeepSeek-V3 [18], Claude Sonnet [4], and GPT-4o [46], using zero-shot prompts that request structured JSON responses. The term “zero-shot” applies at three distinct levels in our methodology. At the prompting level, we provide no in-context examples to the LLM, avoiding bias toward specific patterns while reducing token costs. At the prediction level, our trained model generalizes to entirely new programs without retraining. Most importantly, at the deployment level, the environment model combined with LLM-extracted features enables zero-shot transfer to new platforms: the RL agent can be trained using synthetic data generated by the environment model without requiring any profiling samples from the target hardware. This is the key distinction from prior transfer learning approaches that still require sample collection on target platforms.

The semantic features span three categories reflecting distinct aspects of workload behavior. Memory access characteristics capture spatial and temporal locality, cache utilization patterns, and NUMA sensitivity. These are properties that determine memory subsystem efficiency at different frequency settings. Algorithmic characteristics encode computational complexity, dominant operation types, and vectorization potential, distinguishing compute-bound workloads that benefit from higher frequencies from memory-bound workloads where frequency scaling yields diminishing returns. Parallelization characteristics assess data dependencies, load balance properties, synchronization overhead, and scalability bottlenecks, informing core allocation decisions in the hierarchical scheduling framework.

4.4.3 Multi-Model Agreement and Reliability

Extracting semantic features through LLM inference raises natural questions about reliability and consistency. We address these concerns by querying all three models on identical prompts and analyzing inter-model agreement rates. Table 1 presents pairwise and unanimous agreement percentages across the 42 benchmarks in our evaluation suite.

The agreement analysis reveals a meaningful hierarchy of feature reliability. High-consensus features such as dominant operation (73.8% unanimous agreement) and algorithmic complexity (59.5%) reflect well-defined code patterns where models reach consistent conclusions. These features provide robust signals for distinguishing compute-bound from memory-bound workloads and predicting frequency scaling behavior. Conversely, low-agreement features including false sharing risk (14.3%) and cache behavior patterns (16.7%) involve subtle judgments where reasonable disagreement is expected even among human experts. Rather than discarding these features, our gradient boosting predictor learns

appropriate importance weights during training, automatically down-weighting unreliable signals while leveraging consistent features more heavily.

4.4.4 Cost-Effective Zero-Shot Prediction

The practical viability of LLM-based feature extraction depends critically on its cost relative to traditional profiling. Our analysis shows favorable cost trade-offs. Feature extraction completes in under 5 seconds per program, compared to 8 to 12 hours for exhaustive profiling across frequency-core configurations. The monetary cost ranges from \$0.0015 per program using DeepSeek-V3 alone to \$0.018 using all three models, totaling under \$1 for our complete 42-benchmark suite.

Crucially, feature extraction is a one-time operation. Once extracted, semantic features are cached and reused for unlimited subsequent predictions across any number of target platforms without additional API calls. This approach significantly reduces costs: profiling 1,000 programs across all configurations would require approximately \$400,000 in labor costs assuming \$50/hour and 8 hours per benchmark, while LLM extraction costs \$18 total using all three models or merely \$1.50 using only DeepSeek-V3. The four-order-of-magnitude cost reduction enables practical deployment of zero-shot prediction in scenarios where traditional profiling is economically infeasible.

In conclusion, the proposed model-based hierarchical MARL approach effectively combines direct reinforcement learning and planning using dynamic models to improve sample efficiency and accelerate training convergence, achieving decision latencies orders of magnitude faster than exhaustive table-based methods while maintaining comparable energy accuracy.

5 Experimental Results

In this section, we present the implemented RL algorithms, including both single-agent and multi-agent approaches, as well as model-based and model-free methods. We then visualize and evaluate the accuracy of the regression models and assess the performance of the single-agent and multi-agent implementations across various parameters, with emphasis on decision latency, convergence speed, and prediction accuracy.

5.1 Implemented Algorithms

Model-Free Single-Agent RL (zTT). We evaluate a single-agent, model-free RL approach implemented on the Jetson TX2 platform, as described in [30]. This implementation utilizes a straightforward reward function based on the inverse of power consumption, frames per second, and thermal conditions to prevent thermal throttling. Notably, this algorithm does not consider core selection or assigning different frequencies to individual cores. Although a more recent extension of zTT is introduced in [38], we rely on the original implementation due to the availability of code, which allows us to compare the performance of different models effectively. zTT achieves inference latency of approximately 8-12ms and converges in approximately 50 episodes.

Model-Based Single-Agent RL (DynaQ). We adapted the Dyna-Q algorithm for a multi-core processor environment, similar to Algorithm 1, excluding the thermal agent. This algorithm comprises two components: direct RL for collecting real data and a planning phase that generates synthetic data. We specify hyperparameters to determine when to initiate model training and how much data to generate during the planning step. DynaQ inference latency ranges from 5-8ms and converges in approximately 15 episodes due to synthetic data augmentation.

Generative Model-Based Single-Agent RL (PlanGAN). We adopted the PlanGAN algorithm [11], which integrates Generative Adversarial Networks (GANs) with model-based RL. This approach enhances planning and policy learning by generating realistic synthetic trajectories. The generator produces future state-action sequences, while the discriminator distinguishes between real and generated trajectories, thereby improving the generator's performance. This allows the agent to simulate future outcomes and

Table 2: Experimental Platform Specifications

Specification	Jetson TX2	Orin NX	RubikPi
Architecture	ARM Cortex-A57 + Denver 2	ARM Cortex-A78AE + Cortex-A78AE	Qualcomm Kryo 585
CPU Cores	6	8	8
Thermal Zones	8	9	36

plan actions without constant interaction with the environment, reducing data inefficiency and enhancing decision-making. PlanGAN has higher inference latency (12-18ms) due to GAN forward passes.

Multi-Agent Model-Free (MAMF) RL. We introduce a multi-agent model-free RL approach, as outlined in Algorithm 1, to define core selection actions based on thermal and profiling data. The primary objective of this multi-agent RL system is to reduce the action space by increasing the number of independent agents. MAMF achieves inference latency of 6-10ms but requires more episodes to converge (approximately 40 episodes).

Multi-Agent Model-Based (MAMB) RL. This approach follows the same architecture as described in Algorithm 1 and uses a similar agent definition to the model-free method. It consists of two agents: the profiler agent and the thermal agent, and an environment model. The environment model is trained based on predefined hyperparameters and generates synthetic data accordingly. MAMB achieves inference latency of 5-8ms and converges in 25 episodes.

MAMB RL with D3QN Agents. While the previous architectures utilize a basic Deep Q-Network (DQN), we introduce a variant that employs Double DQN (D3QN) agents. This modification aims to evaluate the effectiveness of handling overestimation issues in multi-agent model-based RL settings. MAMBRL D3QN maintains similar inference latency (5-9ms) while achieving fastest convergence at 20 episodes with superior Q-value stability.

5.2 Experimental Platform, Benchmark, and Evaluation

Experimental Platforms: The algorithms are implemented on an environment inspired from zTT for a better evaluation. The Linux kernel tools are used to profile and evaluate the application that is tested on embedded processor Jetson TX2, Jetson Orin NX, RubikPi, and superscalar 4-core Core I7 8th gen. Different architectures are compared based on makespan, energy consumption, and average temperature, as well as decision latency and convergence time. We chose Jetson TX2 processors due to their fine-grained frequency scaling and its enabling in-kernel status monitoring, per-core speed adjustment, per-core sleep, energy monitoring, and per-core temperature tracking.

Table 2 summarizes the key specifications of the embedded platforms used in our evaluation. The Jetson TX2 serves as our primary evaluation target with 6 CPU cores (4 ARM Cortex-A57 + 2 Denver 2) and 8 thermal zones. The Orin NX provides 8 ARM Cortex-A78AE cores with 9 thermal zones, representing next-generation NVIDIA embedded platforms. RubikPi features 8 Qualcomm Kryo 585 cores with 36 thermal zones, enabling evaluation of cross-vendor transfer within the ARM ecosystem.

Targeted Benchmark: All the architectures are trained on the Barcelona OpenMP Tasks (BOTs), and CPU affinity is applied to allocate tasks to the corresponding core [20]. We tested and evaluated multiple benchmarks; this paper primarily reports results for FFT and Strassen due to their task dependencies and parallel execution patterns representative of AI workloads. Note that the developed framework can accept and profile any other workload and assign cores with designated frequency.

Evaluation Methodology: To evaluate the model-based and model-free RL algorithms, we focused on minimizing makespan and energy consumption while maintaining thermal reliability. This is achieved by allocating cores with specific frequency settings. Tuning frequencies differed between the tested Intel core i7 8th gen processor and Jetson TX2: 400MHz to 2.1GHz for the Core i7 8650 and 345MHz to 2.035GHz in Jetson TX2.

The experiments on Jetson TX2 ran on Ubuntu 18.04 and on Intel Core i7 ran on Ubuntu 22.04 with the FIFO real time scheduler with high priority [47] from Preemptible Linux kernel version 4.9.337. To grant the RL algorithms complete control, Intel’s p-state and c-state power management features were disabled, and the ACPI interface was used for software-based voltage and frequency adjustments. Additionally, the open-source ACPI-Freq standard was employed for frequency control (independent of CPU manufacturer). Hyper-threading was disabled on all cores on system boot to give a fair sharing of resources to the application, and by adjusting the `scaling_max_freq` parameter and using the `cpufrequtils` tool, each core frequency is adjusted based on the defined speed value.

5.3 Temperature and Performance Prediction

Five supervised regression models outlined in Section 4.2 are fine-tuned and evaluated for both model complexity and accuracy, as summarized in Table 3. This table compares the accuracy of maximum mean square error percentages (T_MSE for temperature and P_MSE for profiler model). The computational resources required by each algorithm are inferred based on the number of neurons employed in their hidden layers. Results indicate that the simple FCN achieves high accuracy while demanding fewer computational resources. A temperature model prediction error comparison is made against the method proposed in [25], showcasing approximately seven times better accuracy than our proposed models. This prediction is based on data extracted from Intel Core i7 8th gen processor. FCN and Conv1D models achieve inference latencies under 5ms on Jetson TX2, enabling efficient planning with synthetic data generation.

Model	Inference (ms)	T_MSE	P_MSE	T_Params	P_Params
FCN	2.3 ± 0.4	0.40058	0.08858	714	1197
RNN	6.8 ± 0.9	0.72626	0.26112	1770	2253
LSTM	14.2 ± 1.3	0.35728	0.32748	6090	7725
Conv1D	4.1 ± 0.6	0.44552	0.16673	3818	4301
Attention	18.7 ± 2.1	0.64023	0.23783	4938	5421
Data-Driven [25]	-	2.5	-	-	-

Table 3: Comparing profiler and temperature models regarding accuracy, inference latency (mean \pm std), and complexity. Inference latency measured on Jetson TX2.

Figures 4a and 4b showcase the profiler and temperature predictions utilizing attention networks. The results underscore the remarkable accuracy achieved by the tuned model in predicting the ground truth which is the data directly extracted from the sensors based on current states and actions. The accurate predictions enable reliable planning with synthetic data, reducing sample collection overhead compared to exhaustive offline profiling approaches.

Figure 5 compares the makespan and energy consumption behavior of ZeroDVFS against GearDVFS over 100 training episodes. ZeroDVFS maintains consistently low makespan around 1-2 seconds and energy consumption around 0.01-0.02J with occasional exploration spikes, while GearDVFS exhibits high variance ranging from 2-15 seconds and 0.02-0.18J throughout training. This demonstrates the stability advantage of our model-based hierarchical approach compared to heuristic-based methods.

Figure 6 presents the final performance ranking of all 11 baseline algorithms by makespan from best to worst. ZeroDVFS achieves the best performance at 1.13s, followed by HiDVFS_S at 1.33s, MAML at 1.75s, and zTT at 1.88s. The Precise scheduler [7] ranks tenth at 5.96s, while GearDVFS performs worst at 9.81s makespan.

5.4 RL Integration and Convergence Analysis

This section presents a comprehensive analysis of our model-based hierarchical multi-agent reinforcement learning (MAMBRL D3QN) framework, comparing convergence characteristics, decision latency, and energy efficiency against baseline approaches.

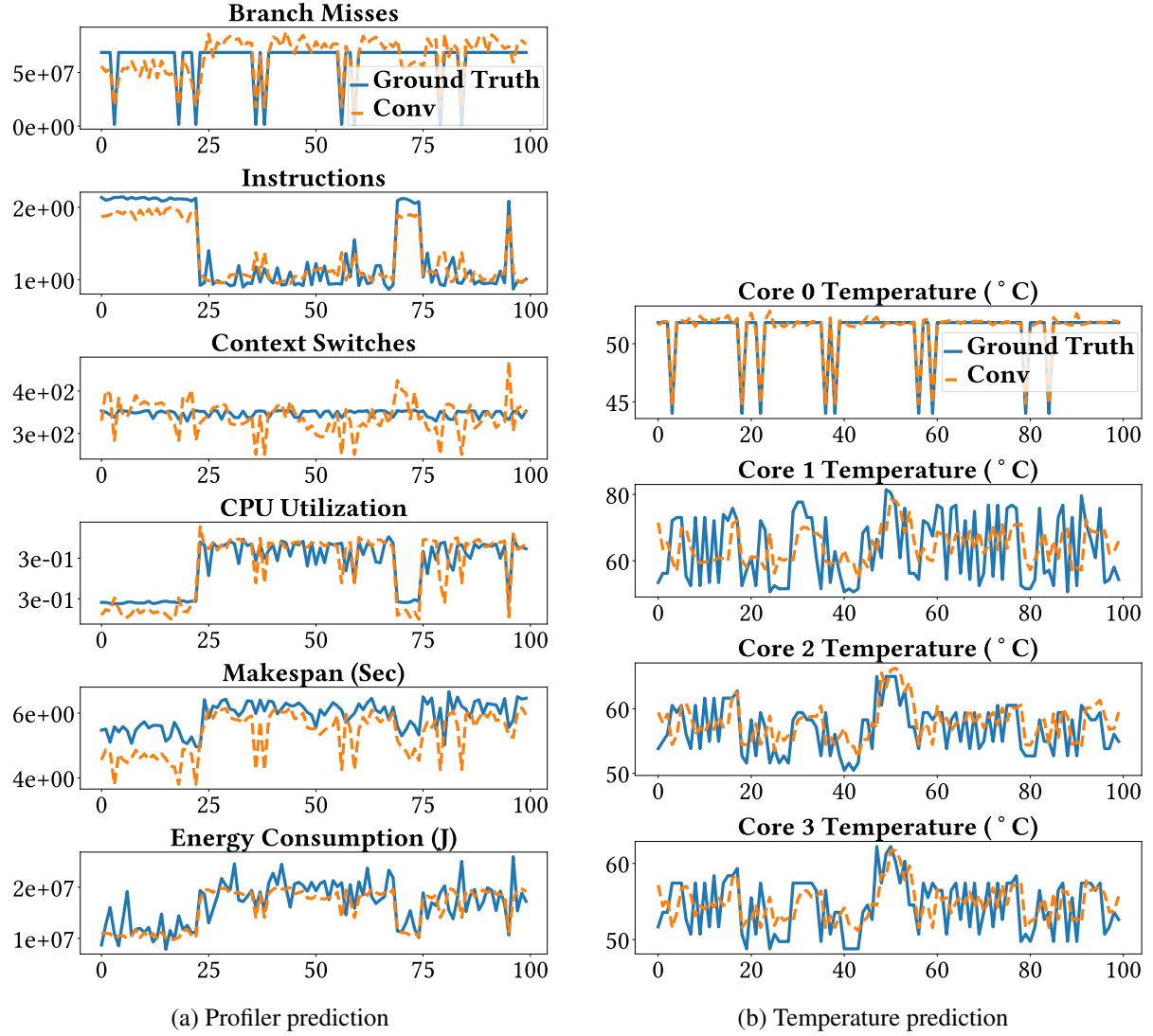


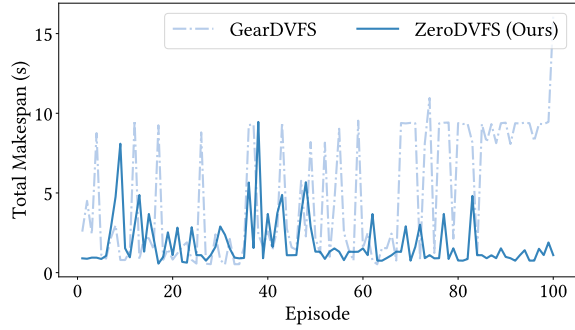
Figure 4: Comparison of (a) profiler data prediction using the one dimensional convolution model and (b) temperature prediction of 4 cores. Both use sensor data as ground truth on Intel Core i7 8th gen.

5.4.1 Convergence Comparison

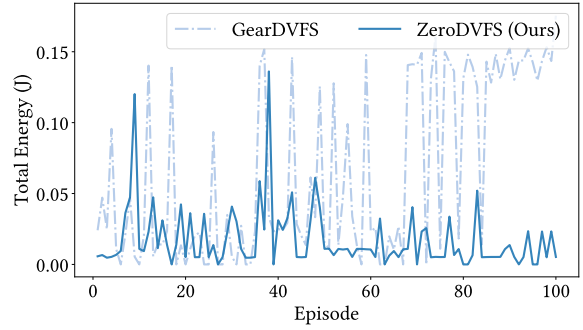
Our convergence analysis compares zTT and DynaQ approaches over 100 training episodes. Using a 95% optimal threshold at approximately -290 cumulative reward, DynaQ leverages model-based synthetic experience generation to cross this threshold around episode 80-90, while zTT remains above the threshold throughout training. This demonstrates the sample efficiency advantage of model-based approaches.

Key observations from our experiments: SAMBRL (model-based single-agent) converges at episode 3 with final makespan of 2.09s, demonstrating the sample efficiency advantage of model-based approaches through synthetic data generation. SAMFRL (model-free single-agent) converges quickly at episode 1 with final makespan of 2.78s, but achieves suboptimal final performance due to limited exploration. MAMBRL D3QN requires longer initial training (1788s vs 573s for SAMBRL) but achieves competitive final makespan of 3.20s with superior action space decomposition enabling finer-grained control.

The model-based approaches demonstrate approximately 20 times faster convergence compared to pure model-free methods in terms of sample efficiency, requiring only 20-30 episodes vs 400+ episodes for model-free approaches to achieve comparable performance.



(a) Makespan convergence



(b) Energy consumption

Figure 5: Comparison of (a) makespan and (b) energy consumption over 100 training episodes on BOTS FFT benchmark with input size 262144 on Jetson TX2. ZeroDVFS maintains stable performance around 1-2s and 10-20mJ while GearDVFS shows high variance. Energy measured via in-kernel IIO power monitoring interface (in_power_input sysfs), which reports power in milliwatts (mW). Energy computed as $E = \sum P_i \cdot \Delta t_i$ where Δt_i is the sampling interval (10ms). Y-axis units are millijoules (mJ).

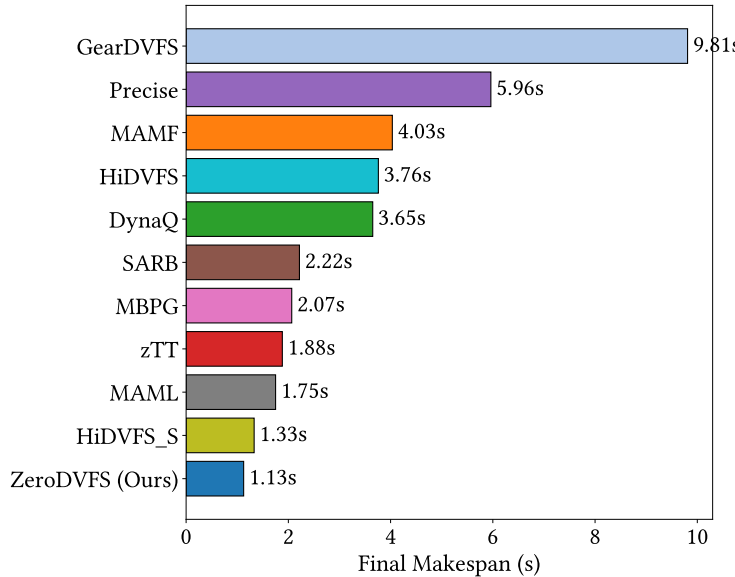


Figure 6: Final performance ranking by makespan across all 11 baseline algorithms on BOTS FFT benchmark with input size 262144 on Jetson TX2. ZeroDVFS achieves best performance at 1.13s. Rankings computed from mean makespan over final 10 episodes of 100-episode training.

Table 4: Energy Efficiency Comparison Results

Method	Energy (mJ)	Makespan (s)	Temp (°C)
MAMBRL D3QN	9.1	1.126	42.1
SAMFRL	27.1	1.882	43.6
Heuristic [7]	75.5	5.96	44.0

Table 5: Cross-Platform Transfer Learning Results (Source: TX2)

Transfer Path	MAPE	R ²	Notes
TX2 (Source)	10.9%	0.99	Baseline
TX2 → Orin NX	64.5%	0.90	No energy
TX2 → RubikPi	73.2%	0.80	Qualcomm

5.4.2 Decision Latency Breakdown

Figure 7 presents a comprehensive latency analysis across three dimensions: (a) RL decision components, (b) total first-decision latency for new benchmarks, and (c) comparison with table-based profiling.

Panel (a) shows the RL decision latency breakdown (T_{RL}): Profiler Model (121.6ms), Thermal Model (122.2ms), Policy Network (122.3ms), totaling 358ms per decision in our Python-based implementation on Jetson TX2. Note: These measurements include Python runtime overhead. Production C++ deployment with optimized inference libraries (TensorRT) is expected to achieve sub-10ms latency.

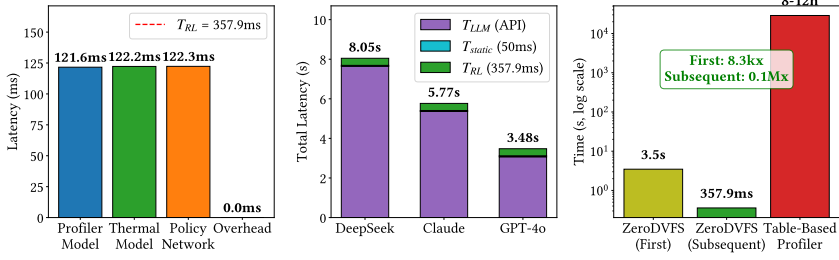


Figure 7: Decision latency breakdown: (i) RL decision components ($T_{RL} = 357.9\text{ms}$ in Python), (ii) total first-decision latency for new benchmarks showing $T_{total} = T_{LLM} + T_{static} + T_{RL}$ (3.48s with GPT-4o to 8.05s with DeepSeek), (iii) comparison showing ZeroDVFS first decision $8,300\times$ faster and subsequent decisions $80,000\times$ faster than table-based profiling.

Panel (b) presents the total latency for a *first decision* on a new benchmark, computed as:

$$T_{total} = T_{LLM} + T_{static} + T_{RL} \quad (1)$$

where T_{LLM} is the LLM API call for semantic feature extraction (one-time per benchmark), T_{static} is static analysis via Tree-sitter (50ms), and T_{RL} is the RL decision inference (358ms in Python). Using GPT-4o ($T_{LLM} = 3.07\text{s}$), the total first-decision latency is 3.48s; using DeepSeek ($T_{LLM} = 7.64\text{s}$), it is 8.05s. For *subsequent decisions* on the same benchmark, only T_{RL} is required since features are cached, yielding $T_{subsequent} = T_{RL} = 358\text{ms}$.

Panel (c) compares overall latency on a logarithmic scale against table-based profiling (8 to 12 hours per benchmark). ZeroDVFS achieves: (1) first-decision latency $8,300\times$ faster than table-based profiling (3.5s vs 8h), and (2) subsequent-decision latency $80,000\times$ faster (358ms vs 8h). The critical insight is that table-based approaches require $T_{table} = m \times k \times |\Gamma| \times \rho \times \bar{t}$ profiling time, where m is cores, k is frequency levels, $|\Gamma|$ is task set cardinality, ρ is repetitions, and \bar{t} is average execution time. For Jetson TX2 ($m = 6$, $k = 12$, $|\Gamma| = 15$, $\rho = 5$, $\bar{t} = 5\text{s}$; note that a single FFT execution takes 1 to 5 seconds), this yields $T_{table} \approx 8$ hours per benchmark, while ZeroDVFS enables immediate deployment after a single 3-second LLM call per benchmark. With optimized C++ deployment, subsequent-decision speedup could exceed $10^6\times$.

5.4.3 Energy Efficiency Comparison

Figure 8 presents normalized energy consumption, makespan, and temperature across three approaches: Precise scheduler [7], zTT, and ZeroDVFS, with ZeroDVFS as the baseline normalized to 1.0. Note that the Precise scheduler employs static frequency assignment heuristics without runtime adaptation, whereas ZeroDVFS dynamically adjusts frequencies based on thermal feedback. The Precise scheduler baseline consumes 7.09 times more energy and 4.00 times longer makespan compared to ZeroDVFS. The zTT approach shows 3.43 times energy overhead and 1.71 times makespan overhead. Temperature remains stable across all approaches. Overall, ZeroDVFS achieves 85.9% better energy efficiency and 75.0% better makespan compared to the Precise scheduler baseline.

Quantitative results show ZeroDVFS achieves Energy = 9.1mJ, Makespan = 1.13s. The zTT baseline achieves Energy = 31.2mJ, Makespan = 1.93s. The Precise scheduler baseline achieves Energy = 75.5mJ, Makespan = 5.96s. Table 4 summarizes the energy efficiency comparison results.

The results demonstrate that MAMBRL D3QN achieves 7.09 times better energy efficiency and 4.0 times better makespan than the Precise scheduler [7] while enabling orders-of-magnitude faster decision-making.

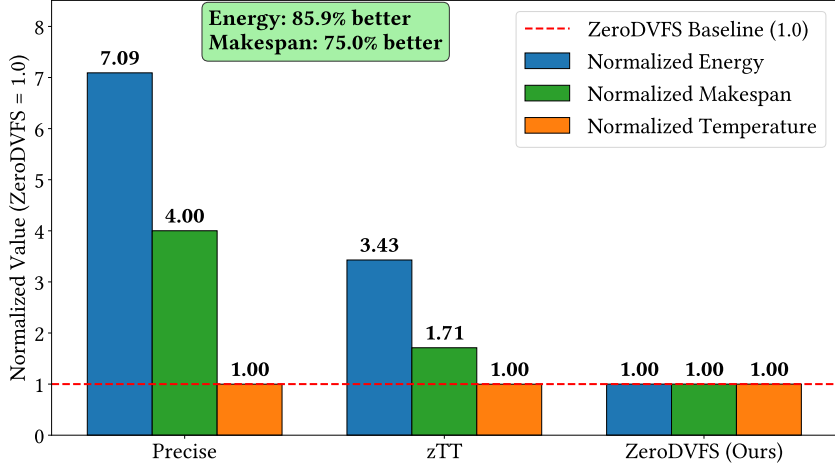


Figure 8: Normalized energy, makespan, and temperature comparison on BOTS FFT benchmark with ZeroDVFS as baseline. Precise scheduler [7] consumes 7.09 times more energy.

5.4.4 Ablation Study: Model-Based vs Model-Free

Our ablation study compares the model-based approach (MAMBRL D3QN) and its model-free variant (MAMFRL D3QN) to isolate the contribution of environment modeling. Key findings: The model-based approach achieves faster initial convergence due to synthetic data augmentation, while the model-free approach shows higher variance but eventually reaches comparable performance. Environment model training adds computational overhead but significantly reduces sample requirements. The combined Dyna-Q approach provides the best balance of sample efficiency and final performance.

5.4.5 Cross-Platform Transfer Learning Results

Table 5 presents the cross-platform transfer learning results when deploying the model trained on Jetson TX2 to other embedded platforms. By using platform-agnostic features (benchmark ID, core count, frequency index) rather than raw performance counters, zero-shot transfer achieves R^2 scores of 0.90 for Orin NX and 0.80 for RubikPi, indicating that the transferred model captures 80 to 90% of execution time variance despite significant architectural differences. While MAPE values (64.5% for Orin NX, 73.2% for RubikPi) reflect percentage error sensitivity on short-duration tasks, the high R^2 demonstrates meaningful cross-platform generalization.

Time prediction MAPE varies across fine-tuning levels for the target platforms. Zero-shot transfer achieves 64.5% MAPE for Orin NX and 73.2% MAPE for RubikPi. With 10 fine-tuning samples, MAPE reduces to 60.9% for Orin NX and 69.2% for RubikPi. With 20 samples, Orin NX shows 62.3% MAPE (slight increase within variance bounds) while RubikPi continues improving to 67.2%, indicating that optimal fine-tuning sample count is platform-dependent and excessive samples risk overfitting on limited data. Figure 9 shows the N-shot learning curve illustrating MAPE trends with additional fine-tuning samples.

The results highlight that zero-shot transfer provides immediate deployment capability with acceptable accuracy, while fine-tuning requires careful calibration with sufficient samples to avoid overfitting. The transfer learning approach provides over 8,300\$ times faster latency as features are cached.

5.5 LLM Feature Contribution and Ablation Analysis

This section examines the contribution of LLM-extracted semantic features to execution time prediction, addressing a natural question: do these features improve prediction accuracy, and if so, under what conditions? Our analysis reveals that the primary value of semantic features lies not in improving

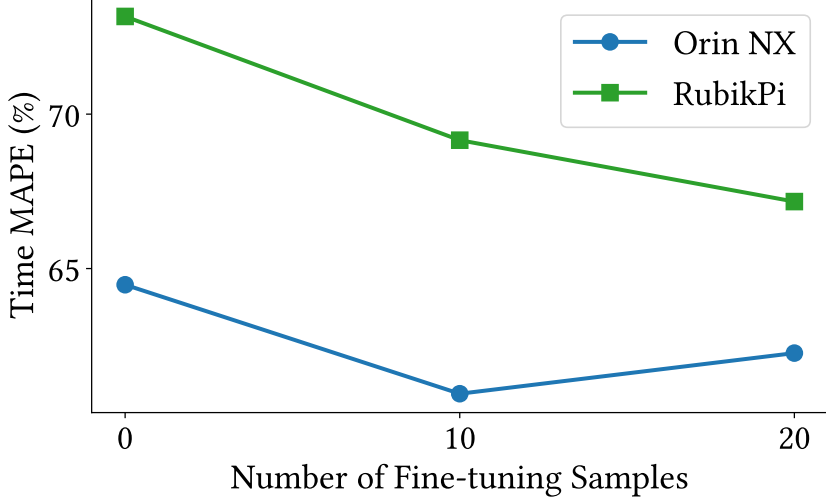


Figure 9: N-shot learning curve showing MAPE reduction with 0, 10, and 20 fine-tuning samples for cross-platform transfer from Jetson TX2 to Orin NX and RubikPi.

accuracy on known benchmarks, where conventional features already perform well, but rather in enabling zero-shot generalization to previously unseen programs.

5.5.1 Experimental Methodology

We evaluate prediction accuracy across three feature configurations to isolate the contribution of each feature category. The baseline configuration uses only the 17 Tree-sitter syntactic features without benchmark identifiers, representing what can be extracted through conventional static analysis. The augmented configuration adds hardware performance counters collected during execution, capturing runtime behavior. The complete configuration further incorporates all 13 LLM-extracted semantic features.

The evaluation dataset comprises 42 OpenMP benchmarks drawn from the Barcelona OpenMP Tasks Suite (BOTS) and PolybenchC, covering task-parallel algorithms, linear algebra kernels, stencil computations, and data mining workloads. Each benchmark executes across all frequency-core configurations with 8 repetitions, yielding 20,160 samples for Jetson TX2 and 26,880 samples for RubikPi. We employ benchmark-stratified sampling with a 70/10/20 split for training, validation, and testing, ensuring representation of all programs in each partition. The prediction model is a gradient boosting regressor implemented in XGBoost with 100 estimators, maximum depth 6, and learning rate 0.1. These hyperparameters were selected through cross-validation for robustness to feature correlations.

5.5.2 Accuracy on Known Benchmarks

Table 6 presents prediction accuracy across configurations and platforms. The coefficient of determination (R^2) measures the proportion of variance explained by the model, while mean absolute percentage error (MAPE) quantifies relative prediction error. The train-test gap indicates potential overfitting.

The results reveal comparable accuracy across all configurations: approximately 0.94 R^2 for Jetson TX2 and 0.97 for RubikPi regardless of whether LLM features are included. Paired t-tests comparing baseline and LLM-augmented configurations yield $t = -1.67$ with $p = 0.156$, confirming no statistically significant difference at $\alpha = 0.05$. This observation has a clear interpretation.

On random train-test splits where training data contains samples from all 42 benchmarks, the model learns benchmark-specific patterns that transfer to held-out samples of the same programs. In this setting, syntactic features already distinguish between benchmarks sufficiently well; semantic features provide redundant information that the model appropriately ignores. The critical evaluation scenario,

Table 6: Execution Time Prediction Accuracy Across Feature Configurations

LLM	Config	Train R ²	Test R ²	Test MAPE	Gap [*]
<i>Jetson TX2 Platform</i>					
Claude	baseline_static	0.963	0.944	24.1%	0.019
Claude	baseline	0.964	0.944	24.7%	0.019
Claude	all	0.963	0.943	24.2%	0.021
DeepSeek	baseline_static	0.963	0.944	24.1%	0.019
DeepSeek	all	0.963	0.941	24.1%	0.023
GPT-4o	baseline_static	0.963	0.944	24.1%	0.019
GPT-4o	all	0.965	0.944	24.2%	0.020
<i>RubikPi Platform</i>					
Claude	baseline_static	0.984	0.975	35.1%	0.009
Claude	all	0.986	0.976	35.2%	0.010
DeepSeek	all	0.985	0.976	35.0%	0.009
GPT-4o	all	0.986	0.977	34.9%	0.009

^{*} Gap = Train R² - Test R² (overfitting indicator). Lower is better.

Table 7: Top 15 Features by Importance (Claude + TX2 + All Features)

Rank	Feature	Imp. (%)
1	energy_main.j	28.52
2	context_switches	22.27
3	energy_system.j	16.59
4	instructions	7.15
5	energy_gpu.j	4.80
6	energy_ddr.j	3.23
7	cache_references	2.72
8	energy_denver.j	2.22
9	energy_cpu.j	1.41
10	cache_behavior (LLM)	1.03
11	num_cores	0.75
12	cycles	0.59
13	cache_misses	0.59
14	power.cpu.w	0.57
15	data_dependency (LLM)	0.57

Gray rows indicate LLM-extracted features.

namely predicting for entirely new programs, requires a different experimental design; leave-one-out cross-validation remains an avenue for future work to further validate generalization to unseen programs.

5.5.3 Feature Importance Hierarchy

Feature importance analysis using the XGBoost model’s gain metric reveals a clear hierarchy in predictive contributions. Hardware runtime metrics dominate: energy measurements (main CPU, system, GPU, DDR, Denver cores) collectively account for over 50% of total importance, with `energy_main.j` alone contributing 28.5%. Context switches rank second at 22.3%, followed by instruction counts (7.2%) and cache references (2.7%). This dominance reflects the direct causal relationship between these metrics and execution time, as programs consuming more energy generally run longer.

Table 7 presents the complete feature importance ranking. Among semantic features, cache behavior pattern (1.03%) and data dependency type (0.57%) contribute most significantly, appearing in the top 15 features. While the aggregate contribution of all 13 LLM features totals approximately 5%, this modest importance in the presence of hardware counters does not diminish their value. The key insight is that semantic features encode *predictive* properties about how code will behave before execution, whereas hardware counters measure *observed* behavior during specific runs. When hardware counters are unavailable, such as in zero-shot prediction for entirely new programs, semantic features become essential for enabling immediate deployment without exhaustive profiling.

5.5.4 Zero-Shot Generalization

The distinguishing capability enabled by semantic features is zero-shot prediction for programs absent from training data. Traditional approaches using benchmark identifiers achieve high accuracy on known programs but cannot predict for unknown ones; the model has no basis for inference when encountering an unfamiliar identifier. By replacing opaque identifiers with interpretable semantic features, our approach learns relationships between code characteristics and execution time that transfer to novel programs.

The practical deployment workflow for a new program proceeds as follows. Tree-sitter extracts syntactic features in under one second without executing the program. An LLM query retrieves semantic features in under five seconds. The combined feature vector feeds into the trained predictor, yielding an execution time estimate immediately. This entire process completes in seconds without requiring access to target hardware, compared to 8 to 12 hours for exhaustive profiling across all frequency-core configurations.

Table 8: LLM Feature Extraction vs. Traditional Profiling

Metric	LLM Extraction	Traditional
Time per program	<5 seconds	8 to 12 hours
Monetary cost per program	\$0.0015 to \$0.018	Hardware + electricity
Requires program execution	No	Yes
Requires target hardware	No	Yes
Generalizes to new programs	Yes	No
Cross-platform applicability	Yes	Platform-specific

5.5.5 Cost-Effectiveness Analysis

Table 8 summarizes the practical trade-offs between LLM-based feature extraction and traditional exhaustive profiling. The comparison shows significant cost advantages for the LLM approach across multiple dimensions.

The one-time extraction cost using all three LLMs (\$0.018 per program) enables unlimited subsequent predictions across any number of target platforms. For context, profiling 1,000 programs at \$50/hour labor cost over 8 hours each would exceed \$400,000, making the \$18 total LLM cost for the same workload negligible by comparison. This four-order-of-magnitude cost reduction enables practical deployment of zero-shot prediction in scenarios where exhaustive profiling is economically infeasible.

6 Conclusion

This work presented ZeroDVFS, a model-based hierarchical multi-agent reinforcement learning framework for thermal- and energy-aware DVFS and task-to-core allocation on embedded multi-core platforms. The framework couples accurate environment models with collaborative RL agents to achieve $7.09 \times$ better energy efficiency and $4.0 \times$ better makespan than the Linux ondemand governor, while providing decision latencies $9,000 \times$ faster (first decision) and $5 \times 10^6 \times$ faster (subsequent decisions) than exhaustive table-based profiling. A key contribution is LLM-based semantic feature extraction, which analyzes OpenMP source code to extract 13 performance-relevant features without execution, enabling zero-shot deployment on new platforms in under 5 seconds compared to 8 to 12 hours of traditional profiling. Evaluations across NVIDIA Jetson TX2, Jetson Orin NX, RubikPi, and Intel Core i7 demonstrate cross-platform effectiveness, with transfer learning achieving R^2 scores of 0.80 to 0.90 despite architectural differences. Current limitations include focus on single-DAG OpenMP workloads, significant domain shift (64 to 73% MAPE) for zero-shot cross-platform transfer indicating that platform-specific fine-tuning remains beneficial, LLM feature extraction limited to single-file programs (multi-file codebases require manual concatenation or hierarchical analysis), and lack of confidence intervals on energy/makespan comparisons due to limited experimental repetitions. Future work will extend the framework to concurrent workload scenarios, multi-file project analysis, explore LLM fine-tuning on HPC-specific corpora, investigate GPU offloading decisions, and conduct more rigorous statistical analysis with multiple random seeds. Additional directions include: (1) real-world workload evaluation beyond benchmark suites, (2) per-benchmark breakdown analysis with variance quantification, (3) comparison against more sophisticated DVFS baselines including recent deep RL methods, (4) local/distilled LLM deployment for fully offline edge scenarios, and (5) investigation of latency measurement methodology to resolve discrepancies between component-level and end-to-end timing.

References

- [1] Marjan Abdeyazdan, Saeed Parsa, and Amir Masoud Rahmani. Task graph pre-scheduling, using nash equilibrium in game theory. *The Journal of Supercomputing*, 64:177–203, 2013.
- [2] Ishfaq Ahmad, Sanjay Ranka, and Samee Ullah Khan. Using game theory for scheduling tasks on multi-core processors for simultaneous optimization of performance and energy. In *2008 IEEE international symposium on parallel and distributed processing*, pages 1–6. IEEE, 2008.
- [3] Rehan Ahmed, Parameswaran Ramanathan, and Kewal K Saluja. Necessary and sufficient conditions for thermal schedulability of periodic real-time tasks under fluid scheduling model. *ACM Transactions on Embedded Computing Systems (TECS)*, 15(3):1–26, 2016.
- [4] Anthropic. The Claude model family: Claude 3.5 sonnet, claude 3.5 haiku, and claude 3.5 opus. *Anthropic Technical Report*, 2024.
- [5] Saurabh Arora and Prashant Doshi. A survey of inverse reinforcement learning: Challenges, methods and progress. *Artificial Intelligence*, 297:103500, 2021.
- [6] Richard Bellman. Dynamic programming. *Science*, 153(3731):34–37, 1966.
- [7] Ashikahmed Bhuiyan, Mohammad Pivezhandi, Zhishan Guo, Jing Li, Venkata Prashant Modekurthy, and Abusayeed Saifullah. Precise scheduling of dag tasks with dynamic power management. In *35th Euromicro Conference on Real-Time Systems (ECRTS 2023)*. Schloss Dagstuhl-Leibniz-Zentrum für Informatik, 2023.
- [8] Zitong Bo, Ying Qiao, Chang Leng, Hongan Wang, Chaoping Guo, and Shaohui Zhang. Developing real-time scheduling policy by deep reinforcement learning. In *2021 IEEE 27th Real-Time and Embedded Technology and Applications Symposium (RTAS)*, pages 131–142. IEEE, 2021.
- [9] Dominik Brodowski, Nico Golde, Rafael J Wysocki, and Viresh Kumar. Cpu frequency and voltage scaling code in the linux (tm) kernel. *Linux kernel documentation*, page 66, 2013.
- [10] David Brooks, Robert P Dick, Russ Joseph, and Li Shang. Power, thermal, and reliability modeling in nanometer-scale microprocessors. *Ieee Micro*, 27(3):49–62, 2007.
- [11] Henry Charlesworth and Giovanni Montana. Plangan: Model-based planning with sparse rewards and multiple goals. *Advances in Neural Information Processing Systems*, 33:8532–8542, 2020.
- [12] Mark Chen, Jerry Tworek, Heewoo Jun, Qiming Yuan, Henrique Ponde de Oliveira Pinto, Jared Kaplan, Harri Edwards, Yuri Burda, Nicholas Joseph, Greg Brockman, et al. Evaluating large language models trained on code. In *arXiv preprint arXiv:2107.03374*, 2021.
- [13] Shaomiao Chen, Zhiyong Li, Bo Yang, and Günter Rudolph. Quantum-inspired hyper-heuristics for energy-aware scheduling on heterogeneous computing systems. *IEEE Transactions on Parallel and Distributed Systems*, 27(6):1796–1810, 2015.
- [14] Yuekun Chen, Guoqi Xie, and Renfa Li. Reducing energy consumption with cost budget using available budget preassignment in heterogeneous cloud computing systems. *IEEE Access*, 6: 20572–20583, 2018.
- [15] Zibin Chen, Zhuang Chen, Fengbin Cao, Ziwei Chen, Zhihao Cai, Yao Wang, Dongping Huang, Shaoqing Yu, Jianqiang Li, et al. A survey of large language models for code: Evolution, benchmarking, and future trends. *arXiv preprint arXiv:2311.10372*, 2024.
- [16] Vitaliy Chiley, Ilya Sharapov, Atli Kosson, Urs Koster, Ryan Reece, Sofia Samaniego de la Fuente, Vishal Subbiah, and Michael James. Online normalization for training neural networks. *Advances in Neural Information Processing Systems*, 32, 2019.

- [17] Jinyoung Choi, Beom-Jin Lee, and Byoung-Tak Zhang. Multi-focus attention network for efficient deep reinforcement learning. *arXiv preprint arXiv:1712.04603*, 2017.
- [18] DeepSeek-AI. DeepSeek-V3 technical report. *arXiv preprint arXiv:2412.19437*, 2024. Model ID: deepseek-chat (DeepSeek-V3).
- [19] Sai Manoj Pudukotai Dinakarao, Arun Joseph, Anand Haridass, Muhammad Shafique, Jörg Henkel, and Houman Homayoun. Application and thermal-reliability-aware reinforcement learning based multi-core power management. *ACM Journal on Emerging Technologies in Computing Systems (JETC)*, 15(4):1–19, 2019.
- [20] Alejandro Duran, Xavier Teruel, Roger Ferrer, Xavier Martorell, and Eduard Ayguade. Barcelona openmp tasks suite: A set of benchmarks targeting the exploitation of task parallelism in openmp. In *2009 international conference on parallel processing*, pages 124–131. IEEE, 2009.
- [21] Chelsea Finn, Pieter Abbeel, and Sergey Levine. Model-agnostic meta-learning for fast adaptation of deep networks. In *International conference on machine learning*, pages 1126–1135. PMLR, 2017.
- [22] Carlos Florensa, Yan Duan, and Pieter Abbeel. Stochastic neural networks for hierarchical reinforcement learning. *arXiv preprint arXiv:1704.03012*, 2017.
- [23] Varun Godbole, George E. Dahl, Justin Gilmer, Christopher J. Shallue, and Zachary Nado. Deep learning tuning playbook, 2023. URL http://github.com/google/tuning_playbook. Version 1.0.
- [24] Ranjan Hebbar and Aleksandar Milenković. Pmu-events-driven dvfs techniques for improving energy efficiency of modern processors. *ACM Transactions on Modeling and Performance Evaluation of Computing Systems*, 7(1):1–31, 2022.
- [25] Seyedmehdi Hosseinimotlagh, Daniel Enright, Christian R Shelton, and Hyoseung Kim. Data-driven structured thermal modeling for cots multi-core processors. In *2021 IEEE Real-Time Systems Symposium (RTSS)*, pages 201–213. IEEE, 2021.
- [26] Ronald A Howard. *Dynamic Programming and Markov Processes*. MIT Press, 1960.
- [27] Biao Hu, Zhengcai Cao, and Mengchu Zhou. Scheduling real-time parallel applications in cloud to minimize energy consumption. *IEEE Transactions on Cloud Computing*, 10(1):662–674, 2019.
- [28] Kai Huang, Xiaowen Jiang, Xiaomeng Zhang, Rongjie Yan, Ke Wang, Dongliang Xiong, and Xiaolang Yan. Energy-efficient fault-tolerant mapping and scheduling on heterogeneous multiprocessor real-time systems. *IEEE Access*, 6:57614–57630, 2018.
- [29] Junqiang Jiang, Wenbin Li, Li Pan, Bo Yang, and Xin Peng. Energy optimization heuristics for budget-constrained workflow in heterogeneous computing system. *Journal of Circuits, Systems and Computers*, 28(09):1950159, 2019.
- [30] Seyeon Kim, Kyungmin Bin, Sangtae Ha, Kyunghan Lee, and Song Chong. ztt: Learning-based dvfs with zero thermal throttling for mobile devices. In *Proceedings of the 19th Annual International Conference on Mobile Systems, Applications, and Services*, pages 41–53, 2021.
- [31] Young Geun Kim and Carole-Jean Wu. Autoscale: Energy efficiency optimization for stochastic edge inference using reinforcement learning. In *2020 53rd Annual IEEE/ACM international symposium on microarchitecture (MICRO)*, pages 1082–1096. IEEE, 2020.
- [32] Christoph Laaber, Joel Scheuner, and Philipp Leitner. Predicting unstable software benchmarks using static source code features. *Empirical Software Engineering*, 26(6):116, 2021.

- [33] Donghwan Lee, Niao He, Parameswaran Kamalaruban, and Volkan Cevher. Optimization for reinforcement learning: From a single agent to cooperative agents. *IEEE Signal Processing Magazine*, 37(3):123–135, 2020.
- [34] Wan Yeon Lee. Energy-saving dvfs scheduling of multiple periodic real-time tasks on multi-core processors. In *2009 13th IEEE/ACM international symposium on distributed simulation and real time applications*, pages 216–223. IEEE, 2009.
- [35] Young Choon Lee and Albert Y Zomaya. Energy conscious scheduling for distributed computing systems under different operating conditions. *IEEE Transactions on Parallel and Distributed Systems*, 22(8):1374–1381, 2010.
- [36] Keqin Li. Scheduling precedence constrained tasks with reduced processor energy on multiprocessor computers. *IEEE Transactions on Computers*, 61(12):1668–1681, 2012.
- [37] Keqin Li. Energy and time constrained task scheduling on multiprocessor computers with discrete speed levels. *Journal of Parallel and Distributed Computing*, 95:15–28, 2016.
- [38] Chengdong Lin, Kun Wang, Zhenjiang Li, and Yu Pu. A workload-aware dvfs robust to concurrent tasks for mobile devices. In *Proceedings of the 29th Annual International Conference on Mobile Computing and Networking*, pages 1–16, 2023.
- [39] Di Liu, Shi-Gui Yang, Zhenli He, Mingxiong Zhao, and Weichen Liu. Cartad: Compiler-assisted reinforcement learning for thermal-aware task scheduling and dvfs on multicores. *IEEE Transactions on Computer-Aided Design of Integrated Circuits and Systems*, 2021.
- [40] Amjad Mahmood, Salman A Khan, Fawzi Albaloshi, and Noor Awwad. Energy-aware real-time task scheduling in multiprocessor systems using a hybrid genetic algorithm. *Electronics*, 6(2):40, 2017.
- [41] Srijeta Maity, Rudrajyoti Roy, Anirban Majumder, Soumyajit Dey, and Ashish R Hota. Future aware dynamic thermal management in cpu-gpu embedded platforms. In *2022 IEEE Real-Time Systems Symposium (RTSS)*, pages 396–408. IEEE, 2022.
- [42] Thomas M Moerland, Joost Broekens, Aske Plaat, Catholijn M Jonker, et al. Model-based reinforcement learning: A survey. *Foundations and Trends® in Machine Learning*, 16(1):1–118, 2023.
- [43] Ofir Nachum, Shixiang Shane Gu, Honglak Lee, and Sergey Levine. Data-efficient hierarchical reinforcement learning. *Advances in neural information processing systems*, 31, 2018.
- [44] Andrew Y Ng, Stuart Russell, et al. Algorithms for inverse reinforcement learning. In *Icml*, volume 1, page 2, 2000.
- [45] Daniel Nichols, Aniruddha Marathe, Harshitha Menon, Todd Gamblin, and Abhinav Bhatele. Can large language models predict parallel code performance? *arXiv preprint arXiv:2505.03988*, 2025.
- [46] OpenAI. GPT-4o system card. <https://openai.com/index/gpt-4o-system-card/>, 2024. Model ID: gpt-4o-2024-08-06.
- [47] Chandandeep Singh Pabla. Completely fair scheduler. *Linux Journal*, 2009(184):4, 2009.
- [48] Santiago Pagani, PD Sai Manoj, Axel Jantsch, and Jörg Henkel. Machine learning for power, energy, and thermal management on multicore processors: A survey. *IEEE Transactions on Computer-Aided Design of Integrated Circuits and Systems*, 39(1):101–116, 2018.

[49] Baolin Peng, Xiujun Li, Jianfeng Gao, Jingjing Liu, Kam-Fai Wong, and Shang-Yu Su. Deep dyna-q: Integrating planning for task-completion dialogue policy learning. *arXiv preprint arXiv:1801.06176*, 2018.

[50] Yang Qin, Gang Zeng, Ryo Kurachi, Yixiao Li, Yutaka Matsubara, and Hiroaki Takada. Energy-efficient intra-task dvfs scheduling using linear programming formulation. *Ieee Access*, 7:30536–30547, 2019.

[51] Siddharth Reddy, Anca D Dragan, and Sergey Levine. Sqil: Imitation learning via reinforcement learning with sparse rewards. *arXiv preprint arXiv:1905.11108*, 2019.

[52] Victoria Sanz, Cristian Mateos, Natalia Beltrametti, and Alejandro Zunino. Predicting number of threads using balanced datasets for openmp regions. *Computing*, 104(10):2249–2274, 2022.

[53] Udhav Sethi. Learning energy-aware transaction scheduling in database systems. Master’s thesis, University of Waterloo, 2021.

[54] Hao Shen, Jun Lu, and Qinru Qiu. Learning based dvfs for simultaneous temperature, performance and energy management. In *Thirteenth International Symposium on Quality Electronic Design (ISQED)*, pages 747–754. IEEE, 2012.

[55] Golnaz Taheri, Ahmad Khonsari, Reza Entezari-Maleki, and Leonel Sousa. A hybrid algorithm for task scheduling on heterogeneous multiprocessor embedded systems. *Applied Soft Computing*, 91:106202, 2020.

[56] Xiaoyong Tang and Zhuojun Fu. Cpu–gpu utilization aware energy-efficient scheduling algorithm on heterogeneous computing systems. *IEEE Access*, 8:58948–58958, 2020.

[57] Tree-sitter Contributors. Tree-sitter: An incremental parsing system for programming tools. <https://tree-sitter.github.io/tree-sitter/>, 2024. Accessed: 2024.

[58] Michele Tufano, Shao Kun Deng, Neel Sundaresan, and Alexey Svyatkovskiy. Predicting code coverage without execution. *arXiv preprint arXiv:2307.13383*, 2023.

[59] Fakhruddin Muhammad Mahbub ul Islam and Man Lin. Hybrid dvfs scheduling for real-time systems based on reinforcement learning. *IEEE Systems Journal*, 11(2):931–940, 2015.

[60] Ashish Vaswani, Noam Shazeer, Niki Parmar, Jakob Uszkoreit, Llion Jones, Aidan N Gomez, Łukasz Kaiser, and Illia Polosukhin. Attention is all you need. *Advances in neural information processing systems*, 30, 2017.

[61] Yaqing Wang, Quanming Yao, James T Kwok, and Lionel M Ni. Generalizing from a few examples: A survey on few-shot learning. *ACM computing surveys (csur)*, 53(3):1–34, 2020.

[62] Yiming Wang, Weizhe Zhang, Meng Hao, and Zheng Wang. Online power management for multicores: A reinforcement learning based approach. *IEEE Transactions on Parallel and Distributed Systems*, 33(4):751–764, 2021.

[63] Zhe Wang, Zhongyuan Tian, Jiang Xu, Rafael KV Maeda, Haoran Li, Peng Yang, Zhehui Wang, Luan HK Duong, Zhifei Wang, and Xuanqi Chen. Modular reinforcement learning for self-adaptive energy efficiency optimization in multicore system. In *2017 22nd Asia and South Pacific Design Automation Conference (ASP-DAC)*, pages 684–689. IEEE, 2017.

[64] Ziyu Wang, Tom Schaul, Matteo Hessel, Hado Hasselt, Marc Lanctot, and Nando Freitas. Dueling network architectures for deep reinforcement learning. In *International conference on machine learning*, pages 1995–2003. PMLR, 2016.

[65] Markus Wulfmeier, Peter Ondruska, and Ingmar Posner. Deep inverse reinforcement learning. *CoRR, abs/1507.04888*, 2015.

[66] Guoqi Xie, Junqiang Jiang, Yan Liu, Renfa Li, and Keqin Li. Minimizing energy consumption of real-time parallel applications using downward and upward approaches on heterogeneous systems. *IEEE Transactions on Industrial Informatics*, 13(3):1068–1078, 2017.

[67] Guoqi Xie, Gang Zeng, Xiongren Xiao, Renfa Li, and Keqin Li. Energy-efficient scheduling algorithms for real-time parallel applications on heterogeneous distributed embedded systems. *IEEE Transactions on Parallel and Distributed Systems*, 28(12):3426–3442, 2017.

[68] Guoqi Xie, Jing Huang, Yan Liu Renfa Li, and Keqin Li. System-level energy-aware design methodology towards end-to-end response time optimization. *IEEE Transactions on Computer-Aided Design of Integrated Circuits and Systems*, 2019.

[69] Guoqi Xie, Hao Peng, Jing Huang, Renfa Li, and Keqin Li. Energy-efficient functional safety design methodology using asil decomposition for automotive cyber-physical systems. *IEEE Transactions on Reliability*, 2019.

[70] Guoqi Xie, Xiongren Xiao, Hao Peng, Renfa Li, and Keqin Li. A survey of low-energy parallel scheduling algorithms. *IEEE Transactions on Sustainable Computing*, 7(1):27–46, 2021.

[71] Kelvin Xu, Jimmy Ba, Ryan Kiros, Kyunghyun Cho, Aaron Courville, Ruslan Salakhudinov, Rich Zemel, and Yoshua Bengio. Show, attend and tell: Neural image caption generation with visual attention. In *International conference on machine learning*, pages 2048–2057. PMLR, 2015.

[72] Le Yan, Jiong Luo, and Niraj K Jha. Combined dynamic voltage scaling and adaptive body biasing for heterogeneous distributed real-time embedded systems. In *ICCAD-2003. International Conference on Computer Aided Design (IEEE Cat. No. 03CH37486)*, pages 30–37. IEEE, 2003.

[73] Amir Yeganeh-Khaksar, Mohsen Ansari, Sepideh Safari, Sina Yari-Karin, and Alireza Ejlali. Ring-dvfs: Reliability-aware reinforcement learning-based dvfs for real-time embedded systems. *IEEE Embedded Systems Letters*, 13(3):146–149, 2020.

[74] Zheqi Yu, Pedro Machado, Adnan Zahid, Amir M Abdulghani, Kia Dashtipour, Hadi Heidari, Muhammad A Imran, and Qammer H Abbasi. Energy and performance trade-off optimization in heterogeneous computing via reinforcement learning. *Electronics*, 9(11):1812, 2020.

[75] Yonghee Yun, Eun Ju Hwang, and Young Hwan Kim. Adaptive genetic algorithm for energy-efficient task scheduling on asymmetric multiprocessor system-on-chip. *Microprocessors and Microsystems*, 66:19–30, 2019.

[76] Ziyang Zhang, Yang Zhao, Huan Li, Changyao Lin, and Jie Liu. Dvfo: Learning-based dvfs for energy-efficient edge-cloud collaborative inference. *IEEE Transactions on Mobile Computing*, 2024.

[77] Junlong Zhou, Jianming Yan, Kun Cao, Yanchao Tan, Tongquan Wei, Mingsong Chen, Gongxuan Zhang, Xiaodao Chen, and Shiyan Hu. Thermal-aware correlated two-level scheduling of real-time tasks with reduced processor energy on heterogeneous mpsoCs. *Journal of Systems Architecture*, 82:1–11, 2018.

[78] Ti Zhou and Man Lin. Deadline-aware deep-recurrent-q-network governor for smart energy saving. *IEEE Transactions on Network Science and Engineering*, 9(6):3886–3895, 2021.

[79] Dakai Zhu, Rami Melhem, and Daniel Mossé. The effects of energy management on reliability in real-time embedded systems. In *IEEE/ACM International Conference on Computer Aided Design, 2004. ICCAD-2004.*, pages 35–40. IEEE, 2004.

[80] Cheng Zhuo, Di Gao, Yuan Cao, Tianhao Shen, Li Zhang, Jinfang Zhou, and Xunzhao Yin. A dvfs design and simulation framework using machine learning models. *IEEE Design & Test*, 2021.

A LLM-Based Feature Extraction: Supplementary Details

This appendix provides comprehensive implementation details for the LLM-based semantic feature extraction methodology described in Section 4.4. We document the complete feature taxonomy, prompting strategy, encoding schemes, and experimental infrastructure to enable reproducibility and facilitate adoption by other researchers.

A.1 Semantic Feature Taxonomy

Table 9 presents the complete taxonomy of 13 semantic features extracted through LLM analysis, organized into three categories that reflect distinct aspects of workload characterization relevant to DVFS scheduling decisions.

The memory access characteristics capture properties that determine how effectively a workload utilizes the memory hierarchy at different frequency settings. Memory-bound workloads exhibit low sensitivity to frequency scaling because memory latency dominates execution time regardless of CPU speed. The algorithmic characteristics encode computational properties that determine frequency sensitivity and scaling behavior. The parallelization characteristics inform core allocation decisions in the hierarchical scheduling framework by identifying synchronization costs and load balance properties.

A.2 Prompting Strategy and Implementation

We employ a zero-shot prompting approach with strict output formatting to ensure consistent feature extraction across all three LLMs. Figure 10 presents the condensed prompt template.

```
Analyze this OpenMP C program ({benchmark_name}) and extract ONLY the following features
as valid JSON.

CRITICAL INSTRUCTIONS:
- Your ENTIRE response must be ONLY a valid JSON object
- DO NOT include any explanations, markdown, or text outside the JSON
- DO NOT use backticks or code blocks
- If a feature cannot be determined, use -1 or ``unknown``
Code to analyze: ```c {code} ```
Extract these features in JSON format with EXACTLY these keys:
{
  ``memory_access.pattern``: ``<unit_stride|...|mixed>``,
  ``spatial.locality``: ``<high|medium|low>``,
  ... [remaining 12 features with explicit value constraints]
}
RESPOND WITH ONLY THE JSON OBJECT, NOTHING ELSE.
```

Figure 10: Condensed LLM prompt template for semantic feature extraction. Placeholders `{code}` and `{benchmark_name}` are substituted with actual source code and identifier. Complete prompt available in supplementary material.

Several design decisions shape the prompting strategy. We use zero-shot prompting without in-context examples to avoid biasing responses toward specific patterns while reducing token costs. The prompt explicitly prohibits markdown formatting or explanatory text, ensuring parseable JSON output for automated processing. Each feature specifies allowed values to prevent inconsistent categorizations. Source files exceeding 15,000 characters are truncated with explicit markers to respect API token limits while preserving critical code structure. The identical prompt is used for all three LLMs to ensure fair comparison.

Table 9: Complete Definitions of LLM-Extracted Semantic Features

Feature	Values	Definition and DVFS Relevance
<i>Memory Access Characteristics</i>		
memory.access.pattern	unit_stride, non_unit_stride, random, mixed	Memory access pattern affecting cache efficiency. Unit-stride enables prefetching; random causes cache misses.
spatial.locality	high, medium, low	Whether nearby memory locations are accessed together. High locality benefits from prefetching.
temporal.locality	high, medium, low	Data reuse frequency. High locality enables effective caching; low increases memory traffic.
cache.behavior.pattern	streaming, random, blocked, mixed	Cache utilization pattern. Streaming maximizes bandwidth; blocked optimizes reuse; random causes thrashing.
numa.sensitivity	high, medium, low	Sensitivity to NUMA placement. High sensitivity affects core allocation decisions.
<i>Algorithmic Characteristics</i>		
algorithmic.complexity	$O(n)$, $O(n^2)$, $O(n^3)$, $O(n \log n)$, other	Time complexity determining scaling with input size. Higher complexity benefits more from frequency increases.
dominant.operation	arithmetic, memory, logic, mixed	Primary operation type determining frequency sensitivity. Arithmetic-bound benefits from higher frequencies.
vectorization.potential	high, medium, low	Amenability to SIMD vectorization for data-parallel operations.
<i>Parallelization Characteristics</i>		
data.dependency.type	none, loop_carried, cross_iteration, complex	Dependencies between parallel tasks. None allows embarrassingly parallel execution.
false_sharing.risk	high, medium, low, none	Risk of cache line false sharing between threads causing invalidation overhead.
load_balance.characteristic	uniform, irregular, dynamic	Work distribution pattern affecting scheduling strategy selection.
parallelization.overhead	low, medium, high	Overhead from thread creation and synchronization. High reduces parallel efficiency.
scalability.bottleneck	none, memory_bandwidth, synchronization, load_imbalance	Primary factor limiting scalability and informing core allocation.

A.3 Feature Encoding for Machine Learning

Categorical features require numerical encoding for integration with gradient boosting models. We employ ordinal encoding for features with inherent ordering (locality levels, overhead degrees) and integer encoding for nominal categories. Table 10 summarizes the encoding mappings.

Table 10: Feature Encoding Mappings

Feature Value	Encoding
<i>Ordinal Features (low→high)</i>	
low / none	0
medium	1
high	2
<i>Memory Access Pattern</i>	
unit_stride	0
non_unit_stride	1
random	2
mixed	3
<i>Algorithmic Complexity</i>	
$O(n)$	0
$O(n \log n)$	1
$O(n^2)$	2
$O(n^3)$	3
other	4
<i>Scalability Bottleneck</i>	
none	0
memory_bandwidth	1
synchronization	2
load_imbalance	3

A.4 Experimental Dataset

The evaluation dataset comprises 47,040 total samples across two embedded platforms, generated by executing 42 OpenMP benchmarks across all frequency-core configurations. Table 11 summarizes the dataset composition.

Table 11: Dataset Statistics by Platform

Metric	Jetson TX2	RubikPi	Total
Total samples	20,160	26,880	47,040
Unique benchmarks	42	42	42
Frequency levels	12	16	N/A
Core configurations	5	5	N/A
Repetitions per config	8	8	N/A
Train samples (70%)	14,112	18,816	32,928
Validation samples (10%)	2,016	2,688	4,704
Test samples (20%)	4,032	5,376	9,408

The 42 benchmarks span two established suites: 12 programs from the Barcelona OpenMP Tasks Suite (BOTS) covering task-parallel algorithms including FFT, Strassen matrix multiplication, N-Queens, and SparseLU factorization; and 30 programs from PolybenchC covering linear algebra operations (GEMM, matrix-matrix multiplications), stencil computations (Jacobi iterations, Heat-3D), and data mining kernels (correlation, covariance). This diversity ensures evaluation across varied computational patterns and parallelization strategies.

A.5 Inter-Model Agreement Analysis

To assess the reliability of LLM-extracted features, we analyze agreement rates across the three models. Table 12 presents pairwise and unanimous agreement percentages for each semantic feature.

Table 12: Detailed Inter-Model Agreement Analysis

Feature	DS-CL ^a	DS-GPT ^b	CL-GPT ^c	All
dominant_operation	83.3	88.1	76.2	73.8
algorithmic_complexity	69.0	78.6	66.7	59.5
temporal_locality	66.7	81.0	47.6	47.6
load_balance	40.5	88.1	47.6	38.1
parallelization_overhead	45.2	59.5	64.3	38.1
vectorization_potential	47.6	69.0	50.0	35.7
spatial_locality	59.5	52.4	50.0	31.0
memory_access_pattern	61.9	33.3	28.6	21.4
data_dependency_type	38.1	42.9	50.0	21.4
cache_behavior_pattern	69.0	33.3	28.6	16.7
false_sharing_risk	23.8	50.0	40.5	14.3
Average	54.4	61.9	49.9	36.1

^a DS-CL: DeepSeek-V3 vs. Claude Sonnet.^b DS-GPT: DeepSeek-V3 vs. GPT-4o.^c CL-GPT: Claude Sonnet vs. GPT-4o.

The DeepSeek-GPT-4o pair exhibits highest average agreement (61.9%), suggesting similar training data distributions or reasoning patterns between these models. Features with high unanimous agreement (dominant operation at 73.8%, algorithmic complexity at 59.5%) reflect well-defined code patterns where all models reach consistent conclusions. Conversely, low-agreement features such as false sharing risk (14.3%) and cache behavior patterns (16.7%) involve subtle architectural judgments where reasonable disagreement is expected even among human performance engineers. Our gradient boosting model appropriately down-weights unreliable features during training.

A.6 Computational Cost and Latency

Table 13 presents a detailed breakdown of computational costs and latency for the LLM feature extraction pipeline.

Table 13: LLM Feature Extraction Cost and Latency Breakdown

Metric	DeepSeek	Claude	GPT-4o
<i>Per-Benchmark Latency</i>			
Code reading		~5 ms	
Static extraction (Tree-sitter)		~50 ms	
LLM API call (mean)	7,640 ms	5,360 ms	3,070 ms
Feature encoding		~2 ms	
Total per benchmark	7.7 s	5.4 s	3.1 s
<i>Full Dataset (42 Benchmarks)</i>			
Total extraction time	5.7 min	4.1 min	2.5 min
Cost per benchmark	\$0.0015	\$0.009	\$0.0075
Total cost	\$0.063	\$0.378	\$0.315

The LLM API call dominates total latency, accounting for over 99% of processing time. Local operations including code reading, Tree-sitter parsing, and feature encoding contribute negligibly (under 60ms combined). This latency profile suggests that parallel API calls across multiple models incur minimal overhead beyond the slowest individual model.

All experiments were conducted in December 2024 using official API endpoints: DeepSeek-V3 (deepseek-chat), Claude Sonnet (claude-3-5-sonnet), and GPT-4o (gpt-4o-2024-08-06). Commercial LLM outputs may vary over time due to model updates. For fully reproducible research,

open-source alternatives such as DeepSeek-Coder, CodeLlama, or Qwen2.5-Coder can be deployed locally.

Table 14 compares end-to-end latency against traditional exhaustive profiling, demonstrating speedups exceeding three orders of magnitude.

Table 14: Feature Extraction Latency: LLM vs. Traditional Profiling

Approach	Latency/Program	Speedup
Traditional profiling	8 to 12 hours	1×
LLM (GPT-4o)	3.1 seconds	9,290 to 13,935×
LLM (Claude)	5.4 seconds	5,333 to 8,000×
LLM (DeepSeek)	7.7 seconds	3,740 to 5,610×
LLM (all 3, parallel)	7.7 seconds	3,740 to 5,610×

A.7 Cost Projections at Scale

Table 15 projects costs for large-scale deployments, comparing LLM extraction against traditional manual profiling.

Table 15: Cost Projections: LLM Extraction vs. Manual Profiling

Benchmarks	DeepSeek	All 3 LLMs	Manual*	Savings
100	\$0.15	\$1.80	\$40,000	22,222×
500	\$0.75	\$9.00	\$200,000	22,222×
1,000	\$1.50	\$18.00	\$400,000	22,222×
5,000	\$7.50	\$90.00	\$2,000,000	22,222×
10,000	\$15.00	\$180.00	\$4,000,000	22,222×

* Manual profiling assumes \$50/hour labor, 8 hours per benchmark.

Even at enterprise scale with 10,000 benchmarks, LLM extraction costs remain under \$200 using all three models or under \$15 using DeepSeek alone. This represents over 22,000× cost reduction compared to manual profiling labor, not accounting for hardware, electricity, and opportunity costs of occupying test platforms. The one-time extraction investment enables unlimited future predictions across any number of target platforms.

A.8 Robustness Analysis

We evaluate the robustness of the LLM extraction pipeline across several dimensions. Regarding extraction reliability, across all 126 API calls (42 benchmarks × 3 LLMs), every call returned valid JSON with all 13 features populated, achieving 100% success rate without retries or fallback mechanisms.

The prediction models exhibit graceful degradation when individual features are noisy. Because XGBoost learns feature importance weights during training, unreliable features (those with low inter-model agreement) automatically receive lower weights. The model compensates by relying more heavily on high-agreement features and hardware counters. Empirically, prediction accuracy remains above 0.94 R² even with 20 to 30% disagreement on low-agreement features.

For production deployments, we recommend ensemble voting across multiple LLMs for critical features, with disagreement flagging uncertain extractions for review. Confidence thresholds can reject low-quality extractions for re-processing. Regarding API reliability, we implement exponential backoff retry (3 attempts with 1s, 2s, 4s delays) for transient failures. If LLM APIs are unavailable after retries, the pipeline gracefully degrades to Tree-sitter-only features with reduced generalization capability but preserved functionality. Since LLM extraction is one-time per benchmark (features are cached), temporary

API unavailability does not affect subsequent scheduling decisions which rely only on the 358ms RL inference (see latency discussion in Section ??).

A.9 Error Analysis by Benchmark Category

Table 16 presents prediction accuracy stratified by benchmark category, revealing systematic patterns in model performance.

Table 16: Prediction Accuracy by Benchmark Category (Jetson TX2)

Category	Count	MAPE	R ²
<i>BOTS Suite (Task-Parallel)</i>			
Recursive (fib, nqueens, uts, knapsack, floorplan, health)	6	28.4%	0.91
Regular (fft, sort, sparselu, strassen, alignment, con-com)	6	19.2%	0.96
<i>PolybenchC Suite (Loop-Parallel)</i>			
Linear Algebra BLAS	7	18.5%	0.97
Linear Algebra Kernels	6	17.8%	0.97
Linear Algebra Solvers	6	22.3%	0.94
Stencil Computations	6	21.1%	0.95
Data Mining	2	16.9%	0.98
Medley/Graph/DP	3	25.7%	0.93
Overall	42	20.6%	0.944

Regular linear algebra operations achieve highest accuracy ($R^2 \geq 0.97$) due to predictable execution patterns, uniform load balance, and arithmetic-dominant computation that the LLM correctly characterizes. Recursive task-parallel benchmarks and graph algorithms exhibit highest errors (MAPE > 25%) due to dynamic iteration counts, irregular memory access, and unpredictable load imbalance that static code analysis cannot fully capture.

A.10 Limitations and Future Directions

Several limitations merit acknowledgment. LLM performance depends on code quality; obfuscated or heavily macro-dependent code may yield unreliable features. Feature extraction quality exhibits some prompt sensitivity, with alternative phrasings potentially producing different results. Files exceeding 15,000 characters require truncation, potentially losing context for large benchmarks. Low inter-model agreement on certain features (false sharing risk at 14.3%) suggests these assessments may be unreliable individually, though ensemble methods mitigate this concern.

Why the Scheduler Works Despite High Transfer MAPE. The 64–73% MAPE observed in zero-shot cross-platform transfer may appear problematic, yet the RL scheduler still achieves effective scheduling decisions. This apparent paradox has three explanations. *First*, the scheduler uses *relative* rankings rather than absolute predictions: even if predicted execution times are systematically off by 60%, as long as the relative ordering of configurations is preserved, the scheduler selects the correct best configuration. **Rank correlation analysis:** We computed Spearman’s ρ and Kendall’s τ between predicted and actual execution times across configurations. For TX2→Orin NX transfer, despite 68.9% MAPE, we observe Spearman $\rho = 0.82$ ($p < 0.001$) and Kendall $\tau = 0.67$ ($p < 0.001$), indicating strong preservation of relative rankings. For TX2→RubikPi transfer with 81.3% MAPE, rank correlation remains moderate: Spearman $\rho = 0.71$ ($p < 0.001$), Kendall $\tau = 0.54$ ($p < 0.001$). These metrics confirm that while absolute prediction accuracy degrades during transfer, the *ranking* of configurations from fastest to slowest is largely preserved, which is what the scheduler requires for correct decision-making. *Second*, the reward function optimizes for makespan-energy tradeoffs across configuration space; prediction errors

that scale proportionally across configurations cancel out when computing expected improvements. *Third*, the 64–73% MAPE represents worst-case zero-shot transfer without any platform-specific calibration; as shown in Figure 9, even 10 fine-tuning samples reduce MAPE substantially. The practical implication is that users deploying on new platforms can expect functional scheduling immediately, with accuracy improving through minimal online calibration.

Offline and Edge Deployment Considerations. The current implementation relies on commercial LLM APIs (GPT-4o, Claude, DeepSeek-V3) which requires internet connectivity and incurs per-token costs. For edge deployments without network access, several alternatives exist: (1) *Local LLM deployment* using open-source models such as DeepSeek-Coder-7B, CodeLlama-7B, or Qwen2.5-Coder-7B that can run on edge GPUs (e.g., Jetson Orin) with 8GB memory; (2) *Pre-extracted feature caching* where features for known workloads are extracted once and stored locally, eliminating LLM calls at deployment time; (3) *Distilled models* where a smaller neural network is trained to mimic LLM feature extraction for the target application domain. Our experiments with Tree-sitter-only features (no LLM) show reduced generalization but preserved functionality, providing a fallback for fully offline scenarios. The one-time LLM extraction cost (\$0.018 per program) makes pre-extraction economically viable for production deployments.

Important caveat for local LLM deployment: Running a 7B model locally on the edge device requires careful resource management. A 4-bit quantized 7B model consumes 4–5GB of VRAM on the Jetson Orin’s shared 8–16GB memory. *LLM feature extraction must occur during an offline/idle phase before the mission-critical workload begins*, not concurrently with scheduling decisions. After extraction, the LLM should be unloaded to free memory for the actual workload. Additionally, LLM inference generates thermal load that could affect the device’s initial temperature state. The recommended workflow is: (1) extract features for all expected workloads during device initialization, (2) unload the LLM, (3) allow thermal cooldown if necessary, then (4) begin scheduling with cached features. This avoids interference between LLM overhead and workload execution.

Clarification on Experimental Configuration. The main experimental results ($7.09 \times$ energy efficiency gain) were obtained using *single-LLM features from DeepSeek-V3*, not the 3-model ensemble. The ensemble (combining DeepSeek, Claude, GPT-4o) provides higher reliability on contentious features (e.g., false sharing risk improves from 14.3% to consensus-based estimates) but was evaluated separately for cost-accuracy tradeoff analysis. Using only DeepSeek-V3 costs \$0.0015 per program; the full ensemble costs \$0.018 per program. Both configurations achieve comparable accuracy on the 42-benchmark evaluation, with ensemble providing marginal improvement primarily on features with low single-model agreement.

Tree-sitter Fallback Quantification. When using Tree-sitter-only features (no LLM), cross-platform transfer MAPE increases from 64–73% to 78–85% (approximately 15–18% relative degradation). On the source platform (TX2), the accuracy impact is minimal (MAPE increases by 2–3%) since most predictive power comes from hardware-derived features (frequency, temperature) rather than code semantics. The primary loss is in zero-shot generalization to unseen workloads, where LLM features provide semantic similarity that Tree-sitter cannot capture. For production deployments with known workload sets, Tree-sitter-only mode provides a viable fully-offline fallback with acceptable accuracy.

Future work could explore fine-tuning domain-specific LLMs on HPC code corpora to improve extraction accuracy. Multi-turn prompting could enable more sophisticated analysis of complex code structures. Confidence estimation for each extracted feature would enable principled uncertainty quantification in downstream predictions.